HHS Public Access

Author manuscript

Cancer Discov. Author manuscript; available in PMC 2022 January 01.

Published in final edited form as:

Cancer Discov. 2021 July ; 11(7): 1826–1843. doi:10.1158/2159-8290.CD-20-1571.

Loss of optineurin drives cancer immune evasion via palmitoylation-dependent IFNGR1 lysosomal sorting and degradation

Wan Du[1,2,9], **Fang Hua**[1,2,9], **Xiong Li**[1,2], **Jian Zhang**[1,2], **Shasha Li**[1,2], **Weichao Wang**[1,2], **Jiajia Zhou**[1,2], **Weimin Wang**[1,2], **Peng Liao**[1,2], **Yijian Yan**[1,2], **Gaopeng Li**[1,2], **Shuang Wei**[1,2], **Sara Grove**[1,2], **Linda Vatan**[1,2], **Witold Zgodziński**[8], **Marek Majewski**[8], **Grzegorz Wallner**[8], **Haoyan Chen**[3], **Ilona Kryczek**[1,2], **Jing-Yuan Fang**[3], **Weiping Zou**[1,2,4,5,6,7,*]

[1]Department of Surgery, University of Michigan School of Medicine, Ann Arbor, MI 48109, USA. [2]Center of Excellence for Cancer Immunology and Immunotherapy, University of Michigan School of Medicine, Ann Arbor, MI 48109, USA. [3]State Key Laboratory for Oncogenes and Related Genes, Key Laboratory of Gastroenterology and Hepatology, Ministry of Health, Division of Gastroenterology and Hepatology, Shanghai Institute of Digestive Disease, Renji Hospital, School of Medicine, Shanghai Jiao Tong University, 145 Middle Shandong Road, Shanghai 200001, China [4]Department of Pathology, University of Michigan School of Medicine, Ann Arbor, MI 48109, USA. [5]Department of Graduate Programs in Immunology, University of Michigan School of Medicine, Ann Arbor, MI 48109, USA. [6]Department of Tumor Biology, University of Michigan School of Medicine, Ann Arbor, MI 48109, USA. [7]University of Michigan Rogel Cancer Center, University of Michigan School of Medicine, Ann Arbor, MI 48109, USA. [8]The 2nd Department of General Surgery, Medical University of Lublin Staszica 16 St., 20-081 Lublin, Poland [9]These authors contributed equally to this work.

Abstract

Mutations in IFN- and MHC-signaling genes endow immunotherapy resistance. Colorectal cancer patients infrequently exhibit IFN- and MHC-signaling gene mutations, and are generally resistant to immunotherapy. In exploring the integrity of the IFN- and MHC-signaling in colorectal cancer, we found that optineurin was a shared node between the two pathways, and predicted colorectal cancer patient outcome. Loss of optineurin occurred in early stage human colorectal cancer. Immunologically, optineurin deficiency attenuated IFNGR1 and MHC-I expression, impaired T

[*]**Correspondence to:** Weiping Zou, M.D., Ph.D. at the Department of Surgery, University of Michigan School of Medicine, 109 Zina Pitcher Place, Ann Arbor, MI, 48109 or at wzou@med.umich.edu, Phone number: 734-615-5554.

AUTHORS' CONTRIBUTIONS

W. Du, **F. Hua**, and **W. Zou** conceived the idea and designed the experiments. **W. Du**, **F. Hua**, and **W. Zou** wrote the manuscript. **W. Du** conducted most experiments with help from **S. Wei**, **S. Grove**, **L. Vatan**, and **J-Y. Fang**; **F. Hua** performed IP-MS, part of the immunohistochemistry experiments, and protein degradation data analysis. **X. Li**, **S. Li**, **H. Chen**, and **J-Y. Fang** contributed to clinical and bioinformatics data analysis. **S. Wei**, **S. Grove**, **J. Zhang**, and **W. Wang** assisted with animal studies, including AOM/DSS animal experiments. **J. Zhou** helped design mutation primers and construct mutated plasmid. **W. Wang** assisted with OT-I cell isolation and co-culture experiments. **P. Liao** helped predict palmitoylation mutant site. **I. Kryczek** assisted with flow cytometry analysis. **Y. Yan** assisted with immunofluorescence experiment. **G. Li** generated reagents. **W. Zgodziński**, **M. Majewski**, and **G. Wallner** provided colorectal cancer tissues and clinic pathological information. **F. Hua**, **I. Kryczek**, and **W. Zou** supervised the study. **W. Zou** acquired funding.

Conflict of interest: W.Z. has served as a scientific advisor for Cstone, Oncopia, and Hengenix.

cell-immunity, and diminished immunotherapy efficacy in murine cancer models and cancer patients. Mechanistically, IFNGR1 was S-palmitoylated on Cys122, and AP3D1 bound with and sorted palmitoylated-IFNGR1 to lysosome for degradation. Unexpectedly, optineurin interacted with AP3D1 to prevent palmitoylated-IFNGR1 lysosomal sorting and degradation - thereby maintaining IFNγ- and MHC-I-signaling integrity. Furthermore, pharmacologically targeting IFNGR1-palmitoylation stabilized IFNGR1, augmented tumor immunity, and sensitized checkpoint therapy. Thus, loss of optineurin drives immune evasion and intrinsic immunotherapy resistance in colorectal cancer.

Keywords

Optineurin; IFNGR1; interferon; MHC; palmitoylation; T cell; PD-1 and PD-L1; AP3D1; colorectal cancer; immunity

INTRODUCTION

Immune therapies induce durable responses across diverse cancers - including melanoma, lung cancer, and bladder cancer (1,2). Colorectal cancer is one of the most frequently diagnosed and fatal cancers worldwide. Approximately 15% of colorectal cancer patients exhibit microsatellite instability-high (MSI-H) or mismatch repair deficient (dMMR) (3–5), and could be sensitive to immune checkpoint therapy (6,7). Hence, the majority of colorectal cancer patients do not respond to current immunotherapy. In order to explore and realize the full potential of immune checkpoint blockade in patients with colorectal cancer, it is essential to identify unknown intrinsic immune evasion and resistance mechanisms in these patients.

Multiple immunosuppressive mechanisms have been demonstrated in the cancer microenvironment (8). Recent compelling evidence has established a connection between genetic and epigenetic alterations and immunotherapy resistance. For example, genetic lesions in the IFN- and antigen-presentation signaling pathways are a defined mechanism for cancer immune evasion and immunotherapy resistance. Mutations in B2M, JAK1, and JAK2, resulting in loss of MHC class I (MHC-I) expression or poor response to IFNγ, are observed in patients with adaptive resistance to immunotherapy (9–11). Meanwhile, copy number alterations in MHC-I and IFNγ-signaling genes are also found in patients with intrinsic resistance to immunotherapy (9–12). Additionally, tumors may evade tumor immunity by impairing effector T cell trafficking into the tumor microenvironment via altered β-catenin signaling (13), epigenetic mechanisms (14,15), and other biological pathways (16–18). While colorectal cancer patients are generally not responsive to immunotherapy, genetic mutations in IFN-signaling pathway and antigen presenting machinery genes are infrequently observed in these patients. For example, B2M mutations are harbored in 3.4% patients with colorectal cancer (19) and JAK1 mutation is found in 5.3% of MSS (Microsatellite Stable) colorectal cancer patients. Therefore, we questioned if there existed broad, yet unknown immunological mechanism(s), which may be fundamentally responsible for immune evasion and intrinsic immunotherapy resistance in patients with colorectal cancer. Given that resistance to the IFNγ- and MHC-I-signaling

pathways is a major immune evasion mechanism (20), in this work we focus on the integrity of the IFNγ- and MHC-I-signaling pathways in patients with colorectal cancer. We found that loss of tumor optineurin expression altered IFNγ receptor 1 (IFNGR1) protein stability and affected the integrity of the IFN-signaling and antigen presenting machinery, as well as T cell-mediated anti-tumor immunity – thereby influencing immunotherapy sensitivity. Thus, loss of optineurin may be a previously unappreciated intrinsic immune evasion and checkpoint blockade resistance mechanism in patients with colorectal cancer.

RESULTS

Tumor optineurin correlates with immunotherapy efficacy and patient outcome

Colorectal cancer patients infrequently exhibit IFN- and MHC-signaling gene mutations. To understand why these patients are generally resistant to immunotherapy, we examined IFN-signaling and antigen presentation gene expression in colorectal cancer and normal colorectal tissues. We initially compared both IFN- and MHC-I-gene signatures in colorectal cancers in The Cancer Genome Atlas Program (TCGA) data set. After stringent filtering criteria, we selected the top 500 genes from each individual gene signature. Among the top 500 genes, 322 genes were shared between IFN- and MHC-I-signaling signatures in colorectal cancers (Fig. 1A). Among these 322 shared genes, we uncovered 15 highly expressed proteins in normal colorectal tissues according to the protein expression score of the Human Protein Atlas (www.proteinatlas.org/pathology) (Fig. 1A). Then, we conducted a proteomic study in 96 paired colon cancer tissues and adjacent normal colon tissues (21). Among the aforementioned 15 proteins, we detected 9 proteins (including optineurin, DDX60, GIMAP1, IFI35, HLA-B, PARP14, SAMD9L, TAP1, and EPSTI1) in the paired colon cancer tissues and adjacent normal colon tissues. Interestingly, optineurin protein levels were decreased in colon cancer tissues as compared to levels in paired normal adjacent tissues, and optineurin was the most often reduced among these 9 proteins, with reduction occurring in 83% of cases (Fig. 1A and Supplementary Table S1). These results were confirmed in an additional colorectal cancer tissue proteomic analysis (22) (Fig. 1B). To directly validate these proteomic results, we assessed optineurin expression with immunohistochemistry staining in colorectal cancer tissues and paired adjacent normal tissues. The intensity of optineurin expression was lower in colorectal cancer tissues than paired adjacent normal tissues (Fig. 1C and Supplementary Fig. S1A). Given that cancer tissues contain tumor cells and different immune cells, we assessed optineurin expression at single cell levels in the human colorectal cancer microenvironment. We first analyzed single cell sequencing data in the human colorectal cancer tissues (23). We found that *optineurin* transcripts were decreased in colorectal cancer epithelial cells as compared to adjacent normal colorectal epithelial cells (Supplementary Fig. S1B). Interestingly, *optineurin* mRNA levels in T cells, B cells, and macrophages were similar in colorectal cancer tissues when compared to adjacent normal colorectal tissues (Supplementary Fig. S1C – E). We next compared optineurin protein levels in paired fresh colorectal cancer tissues and adjacent normal colorectal tissues (Supplementary Fig. S1F – K). Flow cytometry analysis revealed that optineurin protein levels were lower in colorectal cancer epithelial cells when compared to adjacent normal colorectal epithelial cells (Supplementary Fig. S1G), whereas optineurin protein levels in $CD8^+$ T cells, B cells, macrophages, and dendritic cells (DCs) were not

significantly different between the two groups (Supplementary Fig. S1H – K). We extended our studies from colorectal cancer to other types of cancer. Again, we showed reduced levels of *optineurin* transcripts in colorectal cancer, breast cancer, and lung cancer when compared to adjacent normal tissues in TCGA data sets (Supplementary Fig. S1L – N). We next explored the immunological relevance of optineurin in colorectal cancer. Along this line, we found *optineurin* positively correlated with *HLA-A*, *HLA-B*, and *HLA-C* in colorectal cancer (Supplementary Fig. S2A). Similar results were obtained in breast cancer and lung cancer (Supplementary Fig. S2B – C). Altogether, these results suggest that optineurin is a potential immune associated gene and its expression is selectively lost in these human cancers.

To evaluate a potential kinetic alteration of optineurin expression in the course of colorectal cancer development, we included colorectal adenoma in our studies. Similar to colorectal cancer, we found optineurin expression was decreased in colorectal adenoma as compared to normal colorectal tissues (Fig. 1D). The data reveals an early loss of optineurin expression in the progression of colorectal carcinogenesis. Additionally, cancer optineurin expression negatively correlated with colorectal cancer histological grades (Fig. 1E) and advanced TNM stages (Fig. 1F and Supplementary Fig. S2D and E). Furthermore, low expression of cancer optineurin was associated with poor prognosis in patients with colorectal cancer (Fig. 1G and Supplementary Fig. S2F and Supplementary Table S2 and 3). Optineurin expression did not correlate with patient gender, age, and tumor localization (Supplementary Fig. S2G – I). These observations were validated in different colorectal cancer patient cohorts (Fig. 1C – G and Supplementary Fig. S2D – I and Supplementary Table S2 – 5). Patients with melanoma, but not with colorectal cancer, are responsive to checkpoint immunotherapy. In order to explore the clinical significance of optineurin in cancer immunotherapy in cancer patients, we examined the relationship between optineurin protein expression and immunotherapy efficacy in melanoma patients (24). Interestingly, the proteomic analysis demonstrated that clinical benefit rates, including complete response (CR) and partial response (PR), were higher in patients with high levels of optineurin protein expression compared to those with low levels of optineurin protein (Fig. 1H). Moreover, high optineurin protein expression was positively associated with patient survival in melanoma patients treated with anti-PD1 therapy (Fig. 1I). Proteomic and genomic (22) analyses demonstrated that tumor optineurin protein expression failed to correlate with tumor MSI status in patients with colorectal cancer (Supplementary Fig. S2J). Patients with high MSI are sensitive to immunotherapy (7). The data suggest that loss of tumor optineurin expression may be a novel immune evasion mechanism and tumor optineurin is an independent factor determining clinical response to immunotherapy in patients with colorectal cancer. Collectively, loss of optineurin expression correlates with low immune gene signature expression and is associated with poor outcome and immunotherapy resistance in cancer patients.

Optineurin affects tumor immunity and immunotherapy efficacy

Our results suggest that optineurin may play a role in tumor immunity. To test this possibility, we genetically knocked down *optineurin* with specific short hairpin RNAs (shRNAs) (sh-*optineurin*-1 and sh-*optineurin*-2) in murine MC38 colon cancer cells

(Supplementary Fig. S3A). MC38 cells expressing sh-*optineurin* and scramble control similarly proliferated *in vitro* (Supplementary Fig. S3B). We inoculated these cells into NOD-scid IL2Rγ^{null} (NSG) (immune deficient) mice and wild type syngeneic (immune competent) C57/BL6 mice. We observed comparable tumor growth curve, tumor volume, and tumor weight in NSG mice bearing sh-*optineurin* and scramble MC38 tumors (Supplementary Fig. S3C – E). In contrast, sh-*optineurin* expressing MC38 tumor-bearing C57/BL6 mice exhibited faster tumor growth compared with control mice (Fig. 2A). We additionally knocked down *optineurin* in murine CT26 colon cancer cells (Supplementary Fig. S3F) and inoculated these cells into wild type (immune competent) syngeneic Balb/C mice. Again, knocking down tumor *optineurin* resulted in faster CT26 tumor progression (Fig. 2B). To confirm, we constructed *optineurin* knock out (KO) MC38 tumor lines (*optineurin*$^{-/-}$) (Supplementary Fig. S3G) using *optineurin*-specific CRISPR/Cas9 KO plasmid and inoculated these cells into C57/BL6 mice. Similarly, *optineurin* genetic knockout resulted in faster MC38 tumor growth, larger tumor volume, and increased tumor weight compared with control (Fig. 2C – E). To further solidify these data in colitis-associated colorectal cancer model, we crossed floxed *optineurin* (*optineurin*$^{F/F}$) mice with Villin-cre mice and generated intestinal epithelial cell (IEC)-specific *optineurin*-deficient (*optineurin*$^{\Delta IEC}$) mice. We isolated IECs and confirmed specific intestinal epithelial optineurin deletion (Supplementary Fig. S3H). We challenged these mice with azoxymethane (AOM) and dextran sulfate sodium salt (DSS) to induce colorectal tumor development. We found an increase in intestinal tumor numbers and sizes in *optineurin*$^{\Delta IEC}$ (*optineurin*$^{-/-}$) mice as compared to *optineurin*$^{F/F}$ (*optineurin*$^{+/+}$) mice (Fig. 2F and G), whereas the intestinal length was comparable in *optineurin*$^{+/+}$ and *optineurin*$^{-/-}$ mice (Supplementary Fig. S3I). These data indicate that tumor optineurin affects anti-tumor immunity during colorectal tumor development. Differing from Rag1^{tm1Mom} (*Rag1*$^{-/-}$) mice, innate immune cells may be quantitatively and qualitatively impaired in NSG mice due to IL-2 signaling deficiency. To explore whether innate immunity or adaptive immunity was predominantly affected by tumor optineurin expression, we inoculated MC38 colon cancer cells into *Rag1*$^{-/-}$ mice. Similar to the NSG mice, tumor optineurin deficiency did not alter tumor growth, weight, and volume in *Rag1*$^{-/-}$ mice (Supplementary Fig. S3J – L). This result suggests that tumor optineurin affects adaptive immunity in colorectal cancer *in vivo*.

MC38 tumor model is sensitive to PD-L1 and PD-1 blockade (25,26). To test whether tumor optineurin altered MC38 sensitivity to immunotherapy, we treated mice bearing *optineurin* $^{-/-}$ and *optineurin*$^{+/+}$ MC38 tumors with anti-PD-L1 monoclonal antibody (mAb). We found that mice bearing *optineurin*$^{-/-}$ MC38 tumors were less sensitive to anti-PD-L mAb therapy as compared to those bearing *optineurin*$^{+/+}$ MC38 tumors (Fig. 2H). Thus, loss of tumor optineurin drives immune evasion and reduces immunotherapy efficacy.

Optineurin impacts cytotoxic T cell activation and function *in vivo*

To explore the immune mechanism by which loss of tumor optineurin may drive immune evasion, we analyzed immune cell subsets in the tumor microenvironment in mice bearing *optineurin* genetic knock down tumors (Fig. 3A – C and Supplementary Fig. S4A – I) and knock out tumors (Fig. 3D – F and Supplementary Fig. S4J and K). We detected comparable

amounts of tumor infiltrating $CD8^+$ T cells in mice bearing sh-*optineurin* and scramble CT26 tumors (Supplementary Fig. S4B). However, the levels of granzyme B, TNFα, and IFNγ in tumor infiltrating $CD8^+$ (Fig. 3A – C) and $CD4^+$ T cells (Supplementary Fig. S4C – E) were reduced in sh-*optineurin* CT26 tumors, whereas PD-1^+CD8^+ T cells and Tim-3^+CD8^+ T cells were comparable (Supplementary Fig. S4F and G). The levels of IL-2 and Foxp3 in $CD4^+$ T cells (Supplementary Fig. S4H and I) were similar in mice bearing sh-*optineurin* CT26 tumors as compared to mice bearing scramble CT26 tumors. In line with these results, we detected comparable amounts of tumor infiltrating $CD8^+$ T cells in mice bearing *optineurin*$^{-/-}$ and *optineurin*$^{+/+}$ MC38 tumors (Supplementary Fig. S4K). Again, we detected lower levels of granzyme B, TNFα, and IFNγ in tumor infiltrating $CD8^+$ T cells in mice bearing *optineurin*$^{-/-}$ MC38 tumors compared to mice bearing *optineurin*$^{+/+}$ MC38 tumors (Fig. 3D – F). To examine whether optineurin affects cytotoxic T cell activation during colorectal carcinogenesis, we treated *optineurin*$^{F/F}$ (*optineurin*$^{+/+}$) and *optineurin*$^{\Delta IEC}$ (*optineurin*$^{-/-}$) mice with AOM/DSS to induce colorectal tumors. We isolated lamina propria mononuclear cells (LPMCs) from these mice, then analyzed and compared cytotoxic T cell activation. We detected a decrease in granzyme B, TNFα, and IFNγ in $CD8^+$ T cells in *optineurin*$^{-/-}$ mice as compared to *optineurin*$^{+/+}$ mice (Fig. 3G – I). In addition to spontaneous tumor immunity, we also tested if tumor optineurin affected checkpoint blockade-induced $CD8^+$ T cell activation using mice bearing *optineurin*$^{-/-}$ and *optineurin*$^{+/+}$ MC38 tumors (Fig. 3D – F). As expected, anti-PD-L1 mAb therapy enhanced the levels of granzyme B, TNFα, and IFNγ in tumor infiltrating $CD8^+$ T cells in mice bearing *optineurin*$^{+/+}$ MC38 tumors. However, this effect was decreased in mice bearing *optineurin*$^{-/-}$ MC38 tumors (Fig. 3D – F). To explore the clinical relevance of optineurin expression in T cell activation, we examined optineurin expression, T cell activation, and effector T cell signaling proteins in melanoma patients treated with immunotherapy (24). Tumor proteomic analysis demonstrated that optineurin expression positively correlated with T cell activation (Supplementary Fig. S4L) and effector T cell signaling (Fig. 3J) in these patients (24). This result is consistant with our findings in mice bearing optineurin-deficient tumors. Thus, loss of tumor optineurin prevents spontaneous and immunotherapy-induced cytotoxic T cell activation and abolishes anti-tumor immunity.

Optineurin deficiency impairs IFNGR1 expression and antigen presentation

We next examined how optineurin deficiency prevents $CD8^+$ T cell activation. High tumor optineurin expression correlated with MHC-I expression in human colorectal cancer (Fig. 1A and Supplementary Fig. S2A) and T cell activation signaling in melanoma patients (Fig. 3J and Supplementary Fig. S4L). $CD8^+$ T cell activation is mediated by the engagement of TCR to antigen–derived peptide–MHC-I complex. In line with this, we detected a decrease in the *H-2K*^{b} transcripts (Fig. 4A) and mean fluorescence intensity (MFI) of H-$2K^b$ protein (Fig. 4B) in *optineurin*$^{-/-}$ MC38 tumor cells as compared with *optineurin*$^{+/+}$ MC38 tumor cells. This difference persisted in the presence of IFNγ stimulation (Fig. 4A and B). The levels of *HLA-ABC* transcripts were also reduced in *optineurin* knock down human colon cancer LS174T cells (Supplementary Fig. S5A – C). In accordance with the *in vitro* results, the level of H-$2K^b$ protein was also decreased in the IECs in *optineurin*$^{-/-}$ mice compared to that in *optineurin*$^{+/+}$ mice in AOM/DSS model (Fig. 4C). To assess whether optineurin deficiency restricted $CD8^+$ T cell cytotoxic activities due to impaired MHC-I expression, we

cultured mouse ovalbumin (OVA)-specific $CD8^+$ T cells (OT-I) with OVA-expressing *optineurin*$^{-/-}$ and *optineurin*$^{+/+}$ MC38 tumor cells. Tumor optineurin deficiency resulted in a decrease in $CD8^+$ T cell cytotoxic activities, as shown by reduced 7-AAD^+ *optineurin*$^{-/-}$ MC38 tumor cells when compared to *optineurin*$^{+/+}$ MC38 tumor cells (Fig. 4D). This data corresponds with a reduced SIINFEKL-(OVA-peptide)-H-$2k^b$ complex expression in *optineurin*$^{-/-}$ MC38 tumor cells as compared to *optineurin*$^{+/+}$ MC38 tumor cells (Fig. 4E).

We then explored how MHC-I expression was reduced in optineurin deficient tumor cells. Given that MHC-I is often regulated by IFNγ pathway, we assessed the potential relationship between optineurin and the IFNγ pathway. We stimulated tumor cells with IFNγ and observed reduced expression of IFNGR1 protein and STAT1 phosphorylation in sh-*optineurin* LS174T tumor cells (Supplementary Fig. S5D) and optineurin$^{-/-}$ LS174T tumor cells (Supplementary Fig. S5E and F) compared with control cells, indicating that optineurin alters IFNGR1 expression and STAT1 activation. To test if this effect is specific to the IFNγ and STAT1 signaling pathway, we included PD-L1, a well-known IFNγ responsive gene, STAT3, and STAT5 in our experiments. We found IFNγ-induced PD-L1 expression and STAT5 phosphorilation (Supplementary Fig. S5F), and IL-6-induced STAT3 phosphorilation (Supplementary Fig. S5G) were slightly reduced in *optineurin*$^{-/-}$ LS174T tumor cells when compared to wild-type LS174T tumor cells. These results suggest a predominant regulatory role of optineurin on the IFNGR and STAT1 pathway. We inoculated and established *optineurin*$^{-/-}$ MC38, sh-*optineurin* CT26, and control tumors into syngeneic wild type mice. Consistent with the *in vitro* data, immunohistochemistry staining detected a decrease in Ifngr1 expression in *optineurin*$^{-/-}$ MC38 (Supplementary Fig. S5H) and sh-*optineurin* CT26 (Supplementary Fig. S5I) tumor tissues compared with control tissues. The levels of Ifngr1 were also attenuated in *optineurin*$^{-/-}$ IECs as compared to *optineurin*$^{+/+}$ IECs (Supplementary Fig. S5J) isolated from mice AOM/DSS-induced colorectal cancer model (Fig. 2G). These data suggest that optineurin deficiency impairs IFNGR1 expression, thereby affecting the IFNγ signaling pathway. To further support this possibility, we transfected MC38 tumor cells with a GAS (IFNγ-activated site) reporter construct and measured *Stat1* transcriptional activity. Optineurin deficiency caused a decrease in *Stat1* transcriptional activity compared with control cells in response to IFNγ (Supplementary Fig. S5K). To determine the biological role of optineurin in IFNGR1 on $CD8^+$ T cell cytotoxicity, we generated *Ifngr1*$^{-/-}$ MC38 cells. Similar to *optineurin*$^{-/-}$ MC38 cells (Fig. 4E), *Ifngr1*$^{-/-}$ MC38 cells manifested a decrease in SIINFEKL-H-$2k^b$ expression (Fig. 4F) and were resistant to OT-I cell-mediated killing (Fig. 4G). Then, we ectopically expressed *Ifngr1* in wild-type and *optineurin*$^{-/-}$ MC38 cells. We rescued SIINFEKL-H-$2k^b$ expression (Fig. 4H) in *optineurin*$^{-/-}$ tumor cells and recovered their sensitivity to $CD8^+$ T cell killing function (Fig. 4I).

In support of this mouse data, proteomics analysis in human melanoma (24) revealed that optineurin protein expression positively correlated with MHC-I complex and IFNγ-signaling proteins (Fig. 4J). T cell receptor signaling was attenuated in patients with low tumor optineurin expression (24) (Supplementary Fig. S5L). Furthermore, we performed immunohistochemistry staining for IFNGR1 and optineurin in colorectal cancer patients. We detected a positive correlation between IFNGR1 and optineurin in human colorectal cancer tissues (Fig. 4K, Supplementary Fig. S5M). Additionally, the levels of tumor IFNGR1

negatively correlated with colorectal cancer TNM stages (Fig. 4L) and were positively associated with patient survival (Fig. 4M). Thus, loss of optineurin reduces IFNGR1 expression, thereby impairing MHC-antigen presentation and T cell activation, and driving immune escape in cancer.

Loss of optineurin promotes IFNGR1 lysosomal sorting via AP3D1

We explored the molecular mechanism by which optineurin controls IFNGR1 expression. We detected comparable levels of *IFNGR1* mRNA in *optineurin*$^{+/+}$ and *optineurin*$^{-/-}$ LS174T cells (Supplementary Fig. S6A) and mouse MC38 cells (Supplementary Fig. S6B). The data suggests that optineurin may regulate IFNGR1 protein stability, rather than transcripts. To test this possibility, we evaluated the half-life of IFNGR1 in *optineurin*$^{+/+}$ and *optineurin*$^{-/-}$ human colon cancer LS174T cells by blocking *de novo* protein synthesis with cycloheximide (CHX). We found the half-life of IFNGR1 was 3-fold shorter in *optineurin*$^{-/-}$ LS174T cells compared to *optineurin*$^{+/+}$ LS174T cells (Fig. 5A), suggesting that loss of optineurin accelerates IFNGR1 degradation. As monensin blocks intracellular protein transport, we cultured *optineurin*$^{+/+}$ and *optineurin*$^{-/-}$ LS174T cells with monensin to accumulate proteins in the endoplasmic reticulum. Treatment with monensin rescued IFNGR1 protein expression in *optineurin*$^{-/-}$ LS174T cells (Supplementary Fig. S6C). The data further suggests that optineurin may regulate IFNGR1 protein stability, but not *de novo* IFNGR1 protein synthesis. Membrane proteins, including IFNGR1, are often transported to and are degraded in lysosome and/or proteasome (27,28). We treated *optineurin*$^{+/+}$ and *optineurin*$^{-/-}$ LS174T cells with bafilomycin (a lysosome inhibitor) and MG132 (a proteasome inhibitor). Bafilomycin basically (Fig. 5B) and MG132 partially (Supplementary Fig. S6D) rescued IFNGR1 protein expression in optineurin$^{-/-}$ LS174T cells. Thus, IFNGR1 protein may be transported to and is predominantly degraded in lysosomes. We conducted an immunofluorescence staining for IFNGR1 and LAMP1 (a lysosome marker) in *optineurin*$^{+/+}$ and *optineurin*$^{-/-}$ DLD1 cells. As expected, loss of optineurin caused increased IFNGR1 localization in lysosome, as shown by the co-staining of IFNGR1 and LAMP1 (Fig. 5C). The data provides evidence that optineurin deficiency promotes IFNGR1 degradation in lysosomes.

Optineurin is involved in basic cellular functions through interacting with several proteins (29). We posited that optineurin directly interacts with IFNGR1 and regulates its stability. However, immunoprecipitation (IP) experiments failed to detect a direct interaction between optineurin and IFNGR1 in LS174T cells (Supplementary Fig. S6E). To identify potential binding partner(s) of IFNGR1 and optineurin, we performed immunoprecipitation-coupled to mass spectrometry (IP-MS) experiments. Interestingly, we detected that AP3D1 was the most abundant subunit (adaptor related protein complex 3 subunit delta 1) in both IFNGR1-immunoprecipitates (Supplementary Fig. S6F) and optineurin-immunoprecipitates (Supplementary Fig. S6G). Thus, AP3D1 is a potent binding partner of IFNGR1 and optineurin (Supplementary Table S6). AP3D1 is one of the subunits of adaptor protein complex 3 (AP3), which is crucial for selection and trafficking of cargo into lysosomes (30–32). We hypothesized that AP3D1 was involved in IFNGR1 lysosomal sorting for degradation. To test this hypothesis, we knocked down *AP3D1* with specific shRNAs in LS174T cells. As expected, knocking down *AP3D1* resulted in an increase in IFNGR1

protein levels (Supplementary Fig. S6H), and a full rescue of IFNGR1 expression in *optineurin*$^{-/-}$ LS174T cells (Fig. 5D) and optineurin$^{-/-}$ DLD1 cells (Supplementary Fig. S6I). Moreover, knocking-down of *AP3D1* abolished the lysosomal localization of IFNGR1 in *optineurin*$^{-/-}$ DLD-1 cells (Fig. 5E). These results suggest that loss of optineurin accelerates IFNGR1 lysosomal sorting via AP3D1 and subsequent lysosomal degradation.

Given that AP3D1 is a binding partner for both optineurin and IFNGR1, we wondered whether optineurin expression affected the binding of AP3D1 with IFNGR1. IP experiments with anti-AP3D1 and anti-IFNGR1 mAbs revealed higher levels of the IFNGR1-AP3D1 interaction in *optineurin*$^{-/-}$ LS174T cells and *optineurin*$^{-/-}$ DLD1 cells than in their *optineurin*$^{+/+}$ counterparts (Fig. 5F and G and Supplementary Fig. S6J). Consistent with these results, Duolink (IFNGR1-AP3D1) assay showed higher levels of the IFNGR1-AP3D1 interaction in *optineurin*$^{-/-}$ DLD-1 cells (Fig. 5H). Collectively, the data suggest that loss of optineurin facilitates IFNGR1 binding with AP3D1 and heightens AP3D1-mediated-IFNGR1 lysosomal sorting and degradation.

IFNGR1-palmitoylation alters the IFNGR1-AP3D1 interaction and tumor immunity

We dissected the mechanism by which loss of optineurin enhances the AP3D1-IFNGR1 interaction, thereby accelerating IFNGR1 lysosomal sorting and degradation. Lipid modification, including palmitoylation, can regulate the protein–protein interaction (33–36). Some proteins require palmitoylation for adaptor protein recognition and lysosomal sorting (32,37). This prompted us to consider whether IFNGR1 is palmitoylated, and if IFNGR1 palmitoylation facilitates its interaction with AP3D1 for lysosomal sorting and degradation. To test this, we first treated LS174T cells with 2-bromopalmitate (2-BP) (a palmitoylation inhibitor) (Supplementary Fig. S7A) or palmostatin B (a depalmitoylation inhibitor) (Supplementary Fig. S7B). We found 2-BP increased and palmostatin B decreased IFNGR1 protein expression in a time dependent manner (Supplementary Fig. S7A and B). Treatment with 2-BP fully rescued IFNGR1 expression in *optineurin*$^{-/-}$ LS174T cells (Fig. 6A). However, neither optineurin deficiency nor 2-BP treatment had an effect on expression of IL-6 receptor (IL6R) and TNF receptor superfamily member 1A (TNFR1) (Fig. 6A). Click-iT assay detected potent IFNGR1 palmitoylation in *optineurin*$^{-/-}$ LS174T cells (Fig. 6B). We also detected Ifngr1 palmitoylation *in vivo* in *optineurin*$^{-/-}$ tumor cells isolated from AOM/DSS-induced murine colon cancer model (Supplementary Fig. S7C). These data unveil that IFNGR1 expression can be regulated through a previously unknown lipid modification (palmitoylation).

To determine whether IFNGR1 palmitoylation is critical for its interaction with AP3D1 in *optineurin*$^{-/-}$ cells, we treated *optineurin*$^{-/-}$ LS174T cells with 2-BP. Co-IP experiments showed that treatment with 2-BP reduced the interaction between IFNGR1 and AP3D1, and increased IFNGR1 expression in *optineurin*$^{-/-}$ LS174T cells (Fig. 6C). Duolink assay demonstrated that inhibition of palmitoylation with 2-BP attenuated the binding of IFNGR1 to AP3D1 in *optineurin*$^{-/-}$ DLD1 cells (Fig. 6D). These results suggest that the interaction between IFNGR1 and AP3D1 is IFNGR1-palmitoylation dependent. To further validate this possibility, we employed the motif-based predictor MDD-Palm (38) and identified Cys122 as a single conservative palmitoylation site at IFNGR1 (Supplementary Fig. S7D) across

species (Supplementary Fig. S7E). We substituted the Cys122 residue with alanine (C122A) and made an *IFNGR1*^{C122A} mutant through site-directed mutagenesis. This substitution abolished IFNGR1 palmitoylation (Fig. 6E) in *optineurin*$^{-/-}$ LS174T cells, and reduced the IFNGR1-AP3D1 interaction (Fig. 6F and G) in 293T cells (Fig. 6F) and *optineurin*$^{-/-}$ DLD1 cells (Fig. 6G). Therefore, IFNGR1 palmitoylation is required for its interaction with AP3D1.

Palmitoylation can police protein stability (39) and regulate protein lysosomal sorting (32,37). As IFNGR1 degradation occurred in lysosome (Fig. 5), we next explored a connection between IFNGR1 palmitoylation and degradation in the context of optineurin. Indeed, treatment with palmostatin B enhanced the lysosomal localization of IFNGR1 (Supplementary Fig. S7F), whereas treatment with 2-BP reduced IFNGR1 in lysosomes in *optineurin*$^{-/-}$ DLD1 cells and enabled comparable levels of lysosomal-free IFNGR1 in *optineurin*$^{-/-}$ and *optineurin*$^{+/+}$ cells (Supplementary Fig. S7G). The data suggest that IFNGR1 palmitoylation accelerates its lysosomal sorting and degradation. For further confirmation, we treated LS174T cells with palmostatin B to promote IFNGR1 palmitoylation and examined a role of lysosome inhibitor in IFNGR1 degradation. As expected, palmostatin B promoted IFNGR1 degradation and bafilomycin prevented palmitoylation-associated IFNGR1 degradation (Fig. 6H). CHX-chase assay demonstrated that inhibition of palmitoylation delayed IFNGR1 degradation in *optineurin*$^{+/+}$ LS174T cells (Supplementary Fig. S7H). Moreover, *IFNGR1*^{C122A} mutant enhanced IFNGR1 protein stability as compared to scramble control in *optineurin*$^{-/-}$ LS174T cells (Fig. 6I), resembling the effect of 2-BP (Supplementary Fig. S7H). Furthermore, abrogation of palmitoylation with C122A mutation resulted in a decrease in lysosomal IFNGR1 and an increase in lysosomal-free IFNGR1 (Fig. 6J). Thus, IFNGR1 palmitoylation is essential for its interaction with AP3D1 and loss of optineurin results in an accelerated AP3D1-mediated IFNGR1 lysosomal sorting and degradation.

As IFNGR1 palmitoylation is essential for its interaction with AP3D1 and subsequent IFNGR1 lysosomal sorting and degradation, we explored whether suppression of IFNGR1 palmitoylation could restore cancer IFNGR1 expression and sensitize immunotherapy efficacy in preclinical animal model. To this end, we aimed at identifying pharmacological agent(s) that could inhibit both mouse and human protein palmitoylation. Our extensive literature search revealed that cerulenin, a natural product isolated from the fungi *Cephalosporium caerulens*, was capable of inhibiting both mouse and human protein palmitoylation, as shown in RAW264.7 cells and 293T cells (40,41). We treated human and mouse colon cancer cells with cerulenin *in vitro*. Cerulenin inhibited IFNGR1 palmitoylation (Supplementary Fig. S8A and B), and rescued IFNGR1 protein expression in *optineurin*$^{-/-}$ LS174T cells (Supplementary Fig. S8C), sh-*optineurin* CT26 cells (Supplementary Fig. S8D), and *optineurin*$^{-/-}$ primary intestinal epithelial tumor cells isolated from AOM/DSS-induced murine tumor model (Supplementary Fig. S8E). These results prompted us to evaluate a potential anti-tumor effect of cerulenin in cancer immunotherapy setting in preclinical murine model. We treated sh-*optineurin* CT26 tumor-bearing mice with cerulenin in combination with anti-PD-L1 mAb (Fig. 6K). As expected, treatment with anti-PD-L1 alone had minimal effect on tumor growth, while cerulenin treatment alone partially inhibited tumor growth; however, the combination therapy

manifested a synergistic anti-tumor effect, as shown by tumor volume (Fig. 6K) and weight (Fig. 6L) compared with control (Supplementary Fig. S8F). We detected higher levels of tumor H-2D^{d} in mice treated with cerulenin as compared to controls (Supplementary Fig. S8G). Moreover, the combination treatment resulted in high tumor infiltrating CD8^{+} T cell effector function as assessed by granzyme B and TNFα expression (Supplementary Fig. S8H and I). The data suggest that pharmacological inhibition of IFNGR1 palmitoylation may be used in combination with checkpoint blockade to treat patients with poor immunogenic cancers, such as colorectal cancer. As tumor infiltrating APCs and T cells expressed optineurin (Supplementary Fig. S1), we evaluated a potential direct effect of cerulenin on T cells and APCs. We cultured T cells and bone marrow derived macrophages with cerulenin *in vitro*. We found that treatment with cerulenin had no direct effect on T cell activation, as shown by comparable levels of granzyme B, TNFα, and IFNγ expression in CD8^{+} T cells (Supplementary Fig. S8J – L). However, cerulenin enhanced expression of MHC-I (H-2K^{b}) in mouse bone marrow derived macrophages (Supplementary Fig. S8M). Thus, treatment with cerulenin may also target APCs *in vivo*.

DISCUSSION

The remarkable clinical successes of immune checkpoint blockade therapies do not provide therapeutic benefit to the majority of colorectal cancer patients (1,2). Effector T cell–mediated cytotoxicity induces tumor cell death via apoptosis and ferroptosis (42,43). However, tumor associated antigen (TAA)-specific T cell priming and activation can be diminished due to tumor genetic alterations in the IFN signaling and/or antigen-presentation signaling pathways (44–47). Notably, genetic mutations in the IFN- and antigen-presentation pathways infrequently occur in patients with colorectal cancer. We reason that the expressional and functional integrity of the IFN-signaling and antigen presenting gene pathways may ultimately shape cancer immunity and immunotherapy efficacy in patients with colorectal cancer. In line with this concept, our bioinformatics, genetic, proteomic, functional, and model studies have revealed that optineurin transcripts and proteins are consistently reduced in cancer epithelial cells, but not in immune cells, in the colorectal cancer microenvironment. Furthermore, we have detected a gradual loss of optineurin from normal human colorectal tissues to adenoma and colorectal cancer. Although how loss of tumor optineurin occurs in the colorectal cancer microenvironment remains to be defined, it appears that optineurin expression is also reduced in other types of cancer, including breast cancer and lung cancer. Thus, loss of tumor optineurin may be a previously unknown broad immune evasion and checkpoint blockade resistance mechanism in patients with cancer.

Optineurin is defined as an autophagy receptor (48), yet its expression, regulation, and function in the context of immunity, including tumor immunity, is unknown. Genomic, bioinformatic, and proteomic analysis has uncovered optineurin shared in the IFNγ and MHC-I signaling pathways and optineurin protein deficiency emerges in the majority of colon cancer tissues when compared with paired adjacent normal colon tissues. In line with our human data, we have demonstrated that loss of tumor optineurin drives tumor resistance to T cell-mediated tumor killing and results in tumor resistance to treatment with anti-PD-L1 blocking antibodies in AOM/DSS-induced colon cancer model with specific optineurin deficiency in IECs and in several colon tumor cell bearing syngeneic murine models. Given

that colorectal cancer patients are largely not treated with immunotherapy, we have extended our observations to patients with melanoma having received checkpoint therapy (24). We have found that high levels of optineurin protein correlate with increased clinical response to checkpoint therapy in these patients, and are associated with improved patient survival (24). In addition, simultaneous analysis of human colon cancer proteogenomic profile has failed to reveal a correlation of optineurin protein expression with MSI status (22). Patients with MSI-H can be treated with checkpoint therapy due to their high levels of frameshift mutations, leading to potential generation of immunogenic neoantigens (7). Thus, our data suggests that optineurin expression is different from MSI, and could be an immunogenic mechanism and an independent risk factor for determining clinical response to immunotherapy in patients with colorectal cancer. Accordingly, our work not only demonstrates a novel immunological function of optineurin, but also generates compelling evidence that optineurin is a core gene, controlling tumor immune evasion and intrinsic resistance to immunotherapy.

IFNGR1 is essential for the transduction of IFNγ signaling (49). Unexpectedly, IFNGR1, but not IL6R and TNFR1, is rapidly degraded in optineurin deficient colorectal cancer cells. Furthermore, we have demonstrated that IFNGR1 is S-palmitoylated on Cys122 and palmitoylated-IFNGR1 is sorted by adaptor protein AP3D1 to lysosome for degradation. The palmitoylated cysteine in IFNGR1 acts as a signal for AP3D1 recognition and interaction. Consequently, if IFNGR1 harbors such a lysosome sorting signal, there may exist a protective mechanism for IFNGR1 stability to ensure the integrity of the IFNγ-signaling pathway in the human body. Indeed, optineurin functions as an executor to fulfill a protective duty for IFNγ signaling integrity. In line with this notion, we have found optineurin binds to AP3D1 and functions as a blocker to prevent AP3D1-directed lysosomal sorting and degradation of palmitoylated-IFNGR1 (Supplementary Fig. S9). Mechanistically, this palmitoylation-dependent ménage à trois (optineurin-AP3D1-IFNGR1) molecular cascade may serve as a potential model for exploring the biological activities of numerous S-palmitoylation events, but has not been previously reported. In the context of colorectal cancer, early loss of optineurin occurs in patients with adenoma and colorectal cancer, resulting in accelerated IFNGR1 degradation and impaired IFNγ- and MHC-I signaling pathways. Given that AP3D1 recognizes and sorts palmitoylated-IFNGR1 to lysosome for degradation, we sought to target IFNGR1 palmitoylation for colorectal cancer therapy. Supporting this possibility, pharmacological inhibition of palmitoylation can restore IFNGR1 and MHC expression, enhance tumor immunity, and sensitize checkpoint therapy in preclinical model. Our data suggest that this tumor immunity restoration primarily depends on induced IFNGR1 and MHC-I expression on tumor cells. Nonetheless, it remains possible that administration of palmitoylation inhibitor, such as cerulenin, may target not only tumor cells, but also other cells, including APCs.

In summary, our work identifies optineurin as a central molecular node, dually controlling the integrity of the IFNγ− and MHC-I-signaling pathways. Loss of optineurin is a previously unappreciated immune evasion and intrinsic resistance mechanism in colorectal cancer. Additionally, we provide proof of principle that targeting IFNGR1 stability, including palmitoylation, may overcome intrinsic immunotherapy resistance in patients with colorectal cancer.

METHODS

Reagents

Bafilomycin (B1793), cycloheximide (CHX) (C4859), MG132 (474790), 2-BP (238422), palmostatin B (50–873-80001), and SIINFEKL peptide (OVA 257–264) (S7951) were from Sigma-Aldrich. Cerulenin (10005647) was from Cayman Chemicals. Monensin solution (00–4505-51) was from Thermo Fisher. 2-mercaptoethanol (21985023) was from Gibco. Recombinant human IFNγ (285-IF), human IL-6 (206-IL), and mouse IFNγ (485-MI) were from R & D Systems.

Plasmids

Plasmids expressing short hairpin RNAs (shRNA) targeting human optineurin (TRCN0000083746 and TRCN0000430429), mouse optineurin (TRCN0000178154 and TRCN0000182388), and human AP3D1 (TRCN0000298616 and TRCN0000293891) were from Sigma-Aldrich. Double nickase plasmid (h) (sc-401851-NIC), optineurin double nickase plasmid (m) (sc-427990), and control double nickase plasmid (sc-437281) were from Santa Cruz Biotechnology. Mouse Ifngr1 knock-out plasmid was constructed as previously reported (43). Human IFNGR1 (Myc-DDK-tagged) (RC202761), mouse Ifngr1 (Myc-DDK-tagged) (MR226594), human AP3D1 (TurboGFP-tagged) (RG219366), and pCMV6-Entry Tagged Cloning Vector (PS100001) were from OriGene Technologies.

The IFNGR1 C122A mutant plasmid was generated based on human IFNGR1 (Myc-DDK-tagged) (RC202761, Origene) by site-directed mutagenesis using QuikChange II SiteDirected Mutagenesis Kit (200523, Agilent). Specific primers are included in Extended Data Table 7. Plasmids were purified by QIAprep Spin Miniprep Kit (27106, QIAGEN). Plasmids were sequenced to confirm the mutations.

Cell Culture

Human cells (including LS174T, DLD1 and 293T cells) and murine CT26 cells were purchased from the American Type Culture Collection. Murine MC38 cells was as previously reported (25).All cells were cultured at 37°C in a humidified atmosphere containing 5% CO_2. Human LS174T cells were cultured in EMEM medium (30–2003, ATCC). Human DLD1 cells and murine CT26 cells were cultured in RPMI1640 medium (SH3025501, HyClone). Human 293T cells and murine MC38 cells were cultured in DMEM medium (11995065, Gibco). All cell lines were supplemented with 10% FBS (FB61, ASi) and regularly tested for mycoplasma contamination by MycoAlertTM Mycoplasma Detection Kit (LT07–318, LONZA) every 2 weeks. The latest date of the cells tested for mycoplasma contamination was on December 20th, 2020. Cells were thawed at early passage and cultured for up to 12 weeks in total. Splenocytes were obtained from C57BL/6 mice and stimulated with anti-CD3 (2 μg/ml), anti-CD28 (1 μg/ml), IL-2 (10 ng/ml), and 2-mercaptoethanol (50 μM) for 3 days. Bone marrow derived macrophages were obtained from bone marrow after stimulation with GM-CSF (20 ng/ml) for 6 days.

Genetic knockdown and knockout cells

Plasmids expressing short hairpin RNA (shRNA) targeting *optineurin* or scramble sequences were packed into a lentivirus packaging construct and transfected into HEK293T cells with Lipofectamine™ 2000 transfection reagent (11668019, Invitrogen). LS174T, MC38, and CT26 cells were infected with shRNA expressing lentiviruses and selected with 2, 3, and 10 μg/ml puromycin (A1113803, Gibco). Colon cancer cells were transfected with *optineurin* double nickase plasmid (h) (sc-401851-NIC, Santa Cruz), *optineurin* double nickase plasmid (m) (sc-427990, Santa Cruz), or *Ifngr1* KO plasmids. Control double nickase plasmid (sc-437281, Santa Cruz) was used as negative control. Two days later, the transfected cells were cultured in EMEM, RPMI1640, and DMEM complete medium with different concentrations of puromycin for 3 days. Living cells were seeded into 96 well plates with unlimited dilution to reach one cell per well. Knockout clones were validated with Western blot. Plasmids expressing short hairpin RNA (shRNA) targeting *AP3D1* were packed into a lentivirus packaging construct. LS174T and DLD1 cells were infected with AP3D1 shRNA expressing lentiviruses and selected with 2 and 4 μg/ml puromycin to construct AP3D1 knock down and control cells in *optineurin*$^{-/-}$ cells. We transfected mouse *Ifngr1* (Myc-DDK-tagged) vector (MR226594, Origene) and pCMV6-Entry Tagged Cloning Vector (PS100001, Origene) to construct *Ifngr1* overexpressing and control cells in *optineurin*$^{-/-}$ cells. Multiple clones were used for the study.

Animals

Six-to eight-week-old male NSG mice and female C57/BL6, Balb/c, Rag1^{tm1Mom} (Rag1$^{-/-}$), and OT-I C57BL/6-Tg (TcraTcrb) 1100Mjb/J mice (The Jackson Laboratory) were used for this study. All mice were maintained under pathogen-free conditions. *Optineurin* knockdown, knockout, and scramble MC38 cells (3×10^6) or CT26 cells (1×10^5) were subcutaneously injected on the right flank of these mice. Tumor growth was monitored 2 to 3 times per week using calipers fitted with Vernier scale. Tumor volume was calculated as previously described (43). Anti–PD-L1 (clone 53–5.8, Bio X Cell) and IgG1 isotype mAbs were given intraperitoneally at a dose of 100 μg per mouse on day 6 after tumor cell inoculation, then every 3 days for the duration of the experiment. Cerulenin was given intraperitoneally at a dose of 30 mg/kg per mouse on day 7 after tumor cell inoculation, then every 3 days for the duration of the experiment.

Optn$^{tm1a(EUCOMM)Wtsi}$ (MASV; EPD0116_2_G06) mice (Wellcome Trust Sanger Institute, UK) were crossed with B6.129S4-Gt (ROSA)26Sor$^{tm1(FLP1)\ Dym}$/RainJ mice to remove the FRT cassette, including both neo and LacZ, to generate a conditional ready allele (*optineurin*$^{F/F}$). *Optineurin*$^{F/F}$ mice were bred to C57BL/6 mice expressing Cre-recombinase under the control of the villin promoter (The Jackson Laboratory) to generate mice with specific optineurin deficiency in intestinal epithelial cells (IECs) (*optineurin*$^{\Delta IEC}$). Genotypes were determined by PCR. Optineurin$^{F/F}$ (optineurin$^{+/+}$) littermates and *optineurin*$^{\Delta IEC}$ (*optineurin*$^{-/-}$) mice were injected intraperitoneally with 10 mg of AOM (A5486, Sigma-Aldrich) per kilogram body weight. Five days later, 1.5 – 2% DSS (ICN16011080, Fisher scientific) was given in the drinking water for 5 days, followed by regular drinking water for 14–20 days. This cycle was repeated twice. Mice were euthanized

on day 80. All the mouse studies were approved by the Institutional Animal Care and Use Committee at the University of Michigan (PRO00008278).

Cell proliferation assay

Tumor cells were collected and seeded into 96-well plates. To determine the effect of optineurin deficiency on cell growth, 10% volume of alamar Blue (BUF012, Bio-Rad) was added to the medium and incubated for 4 – 6 hours. Absorbance at wavelengths of 570 nm and 600 nm was measured. The percentage difference in reduction between *optineurin*$^{-/-}$ and wild-type (*optineurin*$^{+/+}$) cells was calculated using the following equation: percentage difference between *optineurin*$^{-/-}$ and wild-type (%) = ((117,216 × A570 of treatment) − (80,586 × A600 of treatment)) / ((117,216 × A570 of control) − (80,586 × A600 of control)) × 100 (43).

OT-I cell isolation and co-culture with tumor cells

Splenocytes were isolated from OT-I C57BL/6-Tg (TcraTcrb) 1100Mjb/J. The cells were pelleted, washed, and suspended at 2 ×10^6 cells/ml in RPMI culture medium containing 5 μg/ml OVA257–264 peptides, 10 ng/ml mouse recombinant IL-2, and 50 μM 2-mercaptoethanol. To set up the co-culture of OT-I and OVA$^+$ tumor cells, splenic OT-I cells were magnetically purified by EasySep™ Mouse CD8$^+$ T Cell Isolation Kit (19853, STEMCELL). OT-I cells were activated and collected for co-culture. *Optineurin*$^{+/+}$ and *optineurin*$^{-/-}$ tumor cells were pretreated with OVA peptides (5 μg/ml) for 2 hours. After being washed with PBS, OT-I cells were co-cultured with these tumor cells at a 1:1 ratio for 24 hours. All cells were collected by trypsinization and analyzed by flow cytometry.

Quantitative PCR analysis

Total RNA was extracted using trizol and phenol-chloroform phase separation. cDNA was synthesized using High-Capacity cDNA Reverse Transcription Kit (Thermo Fisher Scientific). Quantitative PCR (qPCR) was performed on cDNA using Fast SYBR Green Master Mix (Thermo Fisher Scientific) on a StepOnePlus™ Real-Time PCR System (Thermo Fisher Scientific). Results are represented as fold change from untreated controls. Primers were purchased from OriGene Technologies. Specific primers are included in Supplementary Table S7.

Luciferase assay

Cells were transfected with a STAT1 homodimer reporter vector (GAS-Luc), negative control, or positive control constructs from the Cignal GAS Reporter Assay Kit (LUC) (CCS-009L, QIAGEN). 24 hours after transfection, luciferase activities were measured using the Dual-Luciferase® Reporter Assay System (TM040, Promega). Promoter activity was normalized to Renilla luciferase activity and expressed as fold change from control.

Immunofluorescence staining and Duo-link assay

Optineurin$^{+/+}$ and *optineurin*$^{-/-}$ DLD1 cells were treated with different experimental conditions, fixed in 4% paraformaldehyde for 15 minutes, and rinsed with PBS three times. Then, these tumor cells were incubated in blocking buffer (3% BSA and 0.01% saponin in

PBS) for 30 minutes at room temperature. The IFNGR1 antibody (GIR-94) (sc-12755, Santa Cruz), LAMP1 antibody (D2D11) (9091, Cell Signaling Technology), or AP3D1 antibody (16454–1-AP, proteintech) were diluted in blocking buffer and incubated overnight at 4°C. The secondary antibodies were diluted in blocking buffer and added to the cells for 1 hour at 37°C. Each step was followed by PBS washing 3 times. DAPI was used to present the nucleus. The cells were finally mounted with anti-fade mounting medium and detected using a confocal laser scanning microscope. The negative control samples were treated with mouse or rabbit IgG antibodies. Duo-link assay (DUO92101, Sigma) was used to demonstrate the interaction between IFNGR1 and AP3D1. Primary antibodies were IFNGR1 (sc-12755, Santa Cruz) and AP3D1 (16454–1-AP, proteintech).

Immunoblotting

Cell lysates were prepared in RIPA Lysis and Extraction Buffer (89901, Thermo Fisher Scientific). The protein concentrations of cell lysates were determined by Pierce™ BCA Protein Assay Kit (23225, Thermo Fisher Scientific). Equivalent amounts of total cellular protein were separated by SDS PAGE and transferred to PVDF membrane (Millipore). Membranes were blocked with 5% w/v non-fat dry milk and incubated with primary antibodies overnight at 4°C, then incubated with HRP-conjugated secondary antibodies for 2 hours at room temperature. Signal was detected using Clarity and Clarity Max Western ECL Blotting Substrates (Bio-Rad) and captured using ChemiDoc Imaging System (Bio-Rad). The proteins were detected with specific antibodies. Quantification of intensity was determined by Gel-Pro.

The following antibodies were used for immunoblotting: anti-optineurin (C-2)(sc-166576, Santa Cruz), anti-IFNGR1 (GIR-94) (sc-12755, Santa Cruz), anti-IL6R (23457–1-AP, Proteintech), anti- TNFR1 (3736T, Cell Signaling Technology), anti-PD-L1 (13684, Cell Signaling Technology), anti-AP3D1 (sc-136277, Santa Cruz for IP) (16454–1-AP, Proteintech for immunoblots), anti-phospho-STAT1 (9167, Cell Signaling Technology), anti-STAT1 (14994, Cell Signaling Technology), anti-phospho-STAT3 (9145, Cell Signaling Technology), anti-STAT3 (12640, Cell Signaling Technology), anti-phospho-STAT5 (4322, Cell Signaling Technology), anti-STAT5 (94205, Cell Signaling Technology), anti-β-actin (D6A8) antibody (8457, Cell Signaling Technology), anti-DYKDDDDK Tag (9A3) (8146, Cell Signaling Technology), and anti-turboGFP (TA150041, Origene).

Immunoprecipitation and mass spectrometry

Co-immunoprecipitation (Co-IP) was performed to verify protein interaction. In brief, cell lysates were incubated with indicated antibodies and Protein A/G Plus-Agarose (Santa Cruz Biotechnology) at 4°C overnight. The immune complex was washed 3 times, then boiled in 2×SDS sample buffer for 10 min. The co-precipitates were resolved using SDS-PAGE and blotted with specific antibodies.

IP-coupled to mass spectrometry (IP-MS) was used for interactive protein identification. DLD-1 cell lysates were incubated with IFNGR1 or optineurin antibodies and Protein A/G Plus-Agarose (Santa Cruz Biotechnology) at 4°C overnight. The immunoprecipitates were resolved using SDS-PAGE and extracted from the gel and subjected to LC-MS/MS

sequencing by QLBio Biotechnology Co., Ltd. In brief, proteins were digested in gel and extracted. The extracted fraction was lyophilized and reconstituted with 20 μl of 2% methanol and 0.1% formic acid for sample loading. The samples were separated with the EASY-nLC 1000 system, which was directly interfaced with the Thermo Orbitrap Fusion mass spectrometer. The mass of peptides was identified by LC-MS/MS Q Exactive™ Hybrid Quadrupole-Orbitrap Mass Spectrometer (Thermo Scientific). The resulting MS/MS data were searched against the human fasta from UniProt using an in-house Proteome Discoverer (Version PD1.4, Thermo-Fisher Scientific). Peptides only assigned to a given protein group were considered unique.

Click-iT identification of palmitoylation

100 μM Click-iT palmitic acid-azide was added to colon cancer cells or the mouse IECs. Cells were incubated at 37°C for 6 hours, then the medium was removed. The cells were washed with PBS before the addition of lysis buffer (1% sodium dodecyl sulfate in 50 mM Tris-HCl, pH 8.0) containing protease and phosphatase inhibitors. The cell lysates were incubated for 30 minutes on ice, sonicated with a probe sonicator, vortexed for 1 minute, and centrifuged at 18,000g at 4°C for 5 minutes. Then, we transferred the supernatants to a tube and determined the protein concentration using the BCA protein assay kit (Thermo Scientific). The protein samples were reacted with biotin-alkyne (764213, Sigma-Aldrich) using the Click-iT Protein Reaction Buffer Kit (C10276, Thermo Fisher Scientific). The biotin alkyne-azide–plamitic-protein complexes were pulled down by streptavidin (20347, Thermo Fisher). The pellets were subjected to immunoblotting for IFNGR1 detection.

Intestinal epithelial cell (IEC) and lamina propria mononuclear cell (LPMC) isolation

IECs were isolated from *optineurin*$^{F/F}$ (*optineurin*$^{+/+}$) and *optineurin*$^{\Delta IEC}$ (*optineurin*$^{-/-}$) mice. Fresh intestinal tissue samples were incubated in 10 ml of PBS with 2 mM EDTA, 0.3% BSA, and 0.2% D-glucose for 15 min at 37°C under slow rotation (200 rpm) in a thermal incubator. Then, tissues were cut and incubated in 10 mL of PBS with 0.02 g collagenase and 10 μL DNase I (10 mg/mL) for 15 min at 37°C under slow rotation (200 rpm) in a thermal incubator. Samples were passed through a 100 μm cell strainer and separated by Ficoll density gradient centrifugation. LPMCs were isolated from the intermedia cells after centrifugation.

Flow cytometry analysis (FACS)

For cell surface MHC-I detection, cells were treated and stained with H-2K^{b} antibody (553570, BD Biosciences) or H-2D^{d} antibody (553580, BD Biosciences) and directly run on a Fortessa flow cytometer (BD Biosciences, San Jose). For cell surface Ifngr1 detection, cells were treated and stained with anti-Ifngr1 (12–1191-82, ThermoFisher). Single cell suspensions were prepared from fresh mouse tumor tissues and lamina propria mononuclear cells (LPMC). Cells were stained with fluorescence conjugated anti-CD45 (560501, BD Biosciences), anti-CD3 (35–0031-82, Thermo Fisher Scientific), anti-CD90 (553004, BD Biosciences), anti-CD4 (17–0042-82, Thermo Fisher Scientific), anti-CD8 (46–0081-82, Thermo Fisher Scientific), anti-EpCAM (17–5791-82, Thermo Fisher Scientific), anti-PD-1 (25–9985-82, Thermo Fisher Scientific) and anti-Tim-3 (747624, BD Biosciences) mAbs. Cytokine expression was determined by intracellular staining. Anti-granzyme B (561142,

BD Biosciences), anti-TNFα (557644, BD Biosciences), anti-IFNγ (563854, BD Biosciences), anti-IL-2 (554429, BD Biosciences), and anti-FOXP3 (560403, BD Biosciences) mAbs were added to immune cells. For *in vivo* experiments, we first gated FSC, then gated single cells (SSC) under FSC population. We gated $CD90^+CD3^+$ cells under SSC population. Then, $CD8^+$ T cells and $CD4^+$ T cells were determined in $CD90^+CD3^+$ T cells. Granzyme B^+, $TNF\alpha^+$ and $IFN\gamma^+$ cells were determined in $CD8^+$ T cell and $CD4^+$ T cell population. IL-2^+ and $FoxP3^+$ cells were determined in $CD4^+$ T cell population. Mouse splenocytes were prepared and stained with anti-CD8 (564983, BD Biosciences), anti-granzyme B (561142, BD Biosciences), anti-TNF (557644, BD Biosciences), and anti-IFNγ (563773, BD Biosciences). Mouse bone marrow derived macrophages were prepared and stained with anti- $H2K^b$ (553570, BD Biosciences). For human optineurin detection, we prepared by staining with anti-optineurin (sc-166576 AF488, Santa Cruz), anti-CD45 (MHCD4530, ThermoFisher), anti-CD3 (562280, BD Biosciences), anti-CD8 (555368, BD Biosciences), anti-CD4 (562424, BD Biosciences), anti-CD19 (25–0198-42, ThermoFisher), anti-CD7 (564020, BD Biosciences), anti-CD33 (561160, BD Biosciences), and anti-CD 11c (559877, BD Biosciences). All samples were read on a Fortessa flow cytometer and data were analyzed with DIVA software (BD Biosciences).

Colorectal cancer specimens

We used paraffin-embedded human colorectal tissue microarrays from three cohorts in this study. Cohorts 1 and 2 were from Shanghai Outdo Biotech. The average follow-up period was 100 months. Cohort 3 was from the Second Department of General Surgery at the Medical University of Lublin between 2001 and 2013. The average follow-up period was 120 months. Clinical and pathological information is listed in Supplementary Tables 2 – 5. The four paired colorectal cancer tissues and adjacent normal colorectal tissues were acquired from The Cooperative Human Tissue Network.

Immunohistochemistry

The tissue section slides were baked for 60 minutes at 60°C, deparaffinized in xylene, and rehydrated through graded concentrations of ethanol in water. The slides were then subjected to antigen retrieval in 1× AR6 buffer (PerkinElmer). Immunohistochemistry staining was performed on a DAKO Autostainer (DAKO, Carpinteria, CA) using DAKO LSAB+ and diaminobenzadine (DAB) as the chromogen. Tissue sections were labeled with optineurin antibody (C-2) (sc-166576, Santa Cruz) or IFNGR1 antibody (10808–1-AP, Proteintech). Sections were left to air-dry, followed by mounting with permanent mounting medium. Expression of optineurin and IFNGR1 was scored using the H-score method (50,51). H-score method took the percentage of positive cells (0–100%) and each staining intensity (0–3+) into account. A final score was calculated on a continuous scale between 0 and 300 using the following formula: H−score = [1× (% cells 1+) +2× (% cells 2+) +3× (% cells 3+)]. Based on the median value of optineurin and IFNGR1 expression, patients were divided into high and low expression groups. Mouse tumor tissues were fixed in 10% formalin and embedded in paraffin. Immunohistochemistry staining was performed using IFNGR1 antibody (10808–1-AP, Proteintech).

Bioinformatics analysis

MHC-I and IFN signaling signatures were obtained from TCGA data set (http://www.cbioportal.org/). The top 500 genes (log FC > 0, P value from small to large) in IFNγ- and MHC-I-signaling gene signatures are listed in Supplementary Table S8. Using The Human Protein Atlas (https://www.proteinatlas.org/), protein expression levels of the overlapping 322 genes between the IFNγ- and MHC-I-signaling gene signatures were analyzed in human normal colorectal tissues based on protein expression score. Based on a single cell sequencing data set (23), optineurin transcrips were analyzed in different cell subsets in the colorectal cancer microenvironment. Protein expression score was defined as high and low expression based on available protein characterization data (21). Specific proteins were detected by proteomic analysis in human colorectal cancer tissues and normal colorectal tissues (21,22), and in melanoma tissues in patients having received anti-PD1 therapy (24). Gene sets represented in the heatmap and GSEA were downloaded from KEGG pathway database and RECTOME database.

Statistical analysis

Statistical analysis was performed using R Language and GraphPad Prism8 software (GraphPad Software, Inc.). Data were shown as mean ± SEM or mean ± SD. Comparisons of measurement data between two groups were performed using two tailed t-tests. Comparison of continuous outcomes across multiple experimental groups was performed using ANOVA models. Pearson correlation was used to evaluate the association between expressions of two genes. Survival functions were estimated by Kaplan–Meier methods. Log-rank test was used to calculate statistical differences. $P < 0.05$ was considered statistically significant.

Supplementary Material

Refer to Web version on PubMed Central for supplementary material.

ACKNOWLEDGEMENTS

We thank Tomasz Maj for intellectual input and discussion.

Financial support: This work was supported in part by the research grants from the U.S. NIH/NCI R01 grants (W.Z) (CA217648, CA123088, CA099985, CA193136, and CA152470), and the NIH through the University of Michigan Rogel Cancer Center Grant (CA46592).

REFERENCES

1. Topalian SL, Drake CG, Pardoll DM. Immune checkpoint blockade: a common denominator approach to cancer therapy. Cancer Cell 2015;27(4):450–61. [PubMed: 25858804]
2. Zou W, Wolchok JD, Chen L. PD-L1 (B7-H1) and PD-1 pathway blockade for cancer therapy: Mechanisms, response biomarkers, and combinations. Sci Transl Med 2016;8(328):328rv4.
3. Gryfe R, Kim H, Hsieh ET, Aronson MD, Holowaty EJ, Bull SB, et al. Tumor microsatellite instability and clinical outcome in young patients with colorectal cancer. N Engl J Med 2000;342(2):69–77. [PubMed: 10631274]
4. Koopman M, Kortman GA, Mekenkamp L, Ligtenberg MJ, Hoogerbrugge N, Antonini NF, et al. Deficient mismatch repair system in patients with sporadic advanced colorectal cancer. Br J Cancer 2009;100(2):266–73. [PubMed: 19165197]

5. Boland CR, Goel A. Microsatellite instability in colorectal cancer. Gastroenterology 2010;138(6):2073–87.e3. [PubMed: 20420947]
6. Le DT, Uram JN, Wang H, Bartlett BR, Kemberling H, Eyring AD, et al. PD-1 Blockade in Tumors with Mismatch-Repair Deficiency. N Engl J Med 2015;372(26):2509–20. [PubMed: 26028255]
7. Le DT, Durham JN, Smith KN, Wang H, Bartlett BR, Aulakh LK, et al. Mismatch repair deficiency predicts response of solid tumors to PD-1 blockade. Science 2017;357(6349):409–13. [PubMed: 28596308]
8. Zou W Immunosuppressive networks in the tumour environment and their therapeutic relevance. Nat Rev Cancer 2005;5(4):263–74. [PubMed: 15776005]
9. Zaretsky JM, Garcia-Diaz A, Shin DS, Escuin-Ordinas H, Hugo W, Hu-Lieskovan S, et al. Mutations Associated with Acquired Resistance to PD-1 Blockade in Melanoma. N Engl J Med 2016;375(9):819–29. [PubMed: 27433843]
10. Sade-Feldman M, Jiao YJ, Chen JH, Rooney MS, Barzily-Rokni M, Eliane JP, et al. Resistance to checkpoint blockade therapy through inactivation of antigen presentation. Nat Commun 2017;8(1):1136. [PubMed: 29070816]
11. Shin DS, Zaretsky JM, Escuin-Ordinas H, Garcia-Diaz A, Hu-Lieskovan S, Kalbasi A, et al. Primary Resistance to PD-1 Blockade Mediated by JAK1/2 Mutations. Cancer Discov 2017;7(2):188–201. [PubMed: 27903500]
12. Gao J, Shi LZ, Zhao H, Chen J, Xiong L, He Q, et al. Loss of IFN-γ Pathway Genes in Tumor Cells as a Mechanism of Resistance to Anti-CTLA-4 Therapy. Cell 2016;167(2):397–404.e9. [PubMed: 27667683]
13. Spranger S, Bao R, Gajewski TF. Melanoma-intrinsic β-catenin signalling prevents anti-tumour immunity. Nature 2015;523(7559):231–5. [PubMed: 25970248]
14. Peng D, Kryczek I, Nagarsheth N, Zhao L, Wei S, Wang W, et al. Epigenetic silencing of TH1-type chemokines shapes tumour immunity and immunotherapy. Nature 2015;527(7577):249–53. [PubMed: 26503055]
15. Sheng W, LaFleur MW, Nguyen TH, Chen S, Chakravarthy A, Conway JR, et al. LSD1 Ablation Stimulates Anti-tumor Immunity and Enables Checkpoint Blockade. Cell 2018;174(3):549–63.e19. [PubMed: 29937226]
16. Manguso RT, Pope HW, Zimmer MD, Brown FD, Yates KB, Miller BC, et al. In vivo CRISPR screening identifies Ptpn2 as a cancer immunotherapy target. Nature 2017;547(7664):413–8. [PubMed: 28723893]
17. Patel SJ, Sanjana NE, Kishton RJ, Eidizadeh A, Vodnala SK, Cam M, et al. Identification of essential genes for cancer immunotherapy. Nature 2017;548(7669):537–42. [PubMed: 28783722]
18. Ishizuka JJ, Manguso RT, Cheruiyot CK, Bi K, Panda A, Iracheta-Vellve A, et al. Loss of ADAR1 in tumours overcomes resistance to immune checkpoint blockade. Nature 2019;565(7737):43–8. [PubMed: 30559380]
19. Middha S, Yaeger R, Shia J, Stadler ZK, King S, Guercio S, et al. Majority of B2M-Mutant and -Deficient Colorectal Carcinomas Achieve Clinical Benefit From Immune Checkpoint Inhibitor Therapy and Are Microsatellite Instability-High. JCO Precis Oncol 2019;3:po.18.00321.
20. Lawson KA, Sousa CM, Zhang X, Kim E, Akthar R, Caumanns JJ, et al. Functional genomic landscape of cancer-intrinsic evasion of killing by T cells. Nature 2020;586(7827):120–6. [PubMed: 32968282]
21. Vasaikar S, Huang C, Wang X, Petyuk VA, Savage SR, Wen B, et al. Proteogenomic Analysis of Human Colon Cancer Reveals New Therapeutic Opportunities. Cell 2019;177(4):1035–49.e19. [PubMed: 31031003]
22. Zhang B, Wang J, Wang X, Zhu J, Liu Q, Shi Z, et al. Proteogenomic characterization of human colon and rectal cancer. Nature 2014;513(7518):382–7. [PubMed: 25043054]
23. Lee HO, Hong Y, Etlioglu HE, Cho YB, Pomella V, Van den Bosch B, et al. Lineage-dependent gene expression programs influence the immune landscape of colorectal cancer. Nat Genet 2020;52(6):594–603. [PubMed: 32451460]
24. Harel M, Ortenberg R, Varanasi SK, Mangalhara KC, Mardamshina M, Markovits E, et al. Proteomics of Melanoma Response to Immunotherapy Reveals Mitochondrial Dependence. Cell 2019;179(1):236–50.e18. [PubMed: 31495571]

25. Lin H, Wei S, Hurt EM, Green MD, Zhao L, Vatan L, et al. Host expression of PD-L1 determines efficacy of PD-L1 pathway blockade-mediated tumor regression. J Clin Invest 2018;128(2):805–15. [PubMed: 29337305]
26. Tang H, Liang Y, Anders RA, Taube JM, Qiu X, Mulgaonkar A, et al. PD-L1 on host cells is essential for PD-L1 blockade-mediated tumor regression. J Clin Invest 2018;128(2):580–8. [PubMed: 29337303]
27. Kurten RC, Cadena DL, Gill GN. Enhanced degradation of EGF receptors by a sorting nexin, SNX1. Science 1996;272(5264):1008–10. [PubMed: 8638121]
28. Meng X, Liu X, Guo X, Jiang S, Chen T, Hu Z, et al. FBXO38 mediates PD-1 ubiquitination and regulates anti-tumour immunity of T cells. Nature 2018;564(7734):130–5. [PubMed: 30487606]
29. Ying H, Yue BY. Cellular and molecular biology of optineurin. Int Rev Cell Mol Biol 2012;294:223–58. [PubMed: 22364875]
30. Simpson F, Peden AA, Christopoulou L, Robinson MS. Characterization of the adaptor-related protein complex, AP-3. J Cell Biol 1997;137(4):835–45. [PubMed: 9151686]
31. Andrzejewska Z, Névo N, Thomas L, Bailleux A, Chauvet V, Benmerah A, et al. Lysosomal Targeting of Cystinosin Requires AP-3. Traffic 2015;16(7):712–26. [PubMed: 25753619]
32. Bagh MB, Peng S, Chandra G, Zhang Z, Singh SP, Pattabiraman N, et al. Misrouting of v-ATPase subunit V0a1 dysregulates lysosomal acidification in a neurodegenerative lysosomal storage disease model. Nat Commun 2017;8:14612. [PubMed: 28266544]
33. Greaves J, Chamberlain LH. Palmitoylation-dependent protein sorting. J Cell Biol 2007;176(3):249–54. [PubMed: 17242068]
34. Zhang MM, Hang HC. Protein S-palmitoylation in cellular differentiation. Biochem Soc Trans 2017;45(1):275–85. [PubMed: 28202682]
35. Fukata Y, Fukata M. Protein palmitoylation in neuronal development and synaptic plasticity. Nat Rev Neurosci 2010;11(3):161–75. [PubMed: 20168314]
36. Shipston MJ. Ion channel regulation by protein palmitoylation. J Biol Chem 2011;286(11):8709–16. [PubMed: 21216969]
37. Canto I, Trejo J. Palmitoylation of protease-activated receptor-1 regulates adaptor protein complex-2 and -3 interaction with tyrosine-based motifs and endocytic sorting. J Biol Chem 2013;288(22):15900–12. [PubMed: 23580642]
38. Weng SL, Kao HJ, Huang CH, Lee TY. MDD-Palm: Identification of protein S-palmitoylation sites with substrate motifs based on maximal dependence decomposition. PLoS One 2017;12(6):e0179529. [PubMed: 28662047]
39. Linder ME, Deschenes RJ. Palmitoylation: policing protein stability and traffic. Nat Rev Mol Cell Biol 2007;8(1):74–84. [PubMed: 17183362]
40. Lu Y, Zheng Y, Coyaud É, Zhang C, Selvabaskaran A, Yu Y, et al. Palmitoylation of NOD1 and NOD2 is required for bacterial sensing. Science 2019;366(6464):460–7. [PubMed: 31649195]
41. Kim YC, Lee SE, Kim SK, Jang HD, Hwang I, Jin S, et al. Toll-like receptor mediated inflammation requires FASN-dependent MYD88 palmitoylation. Nat Chem Biol 2019;15(9):907–16. [PubMed: 31427815]
42. Barry M, Bleackley RC. Cytotoxic T lymphocytes: all roads lead to death. Nat Rev Immunol 2002;2(6):401–9. [PubMed: 12093006]
43. Wang W, Green M, Choi JE, Gijón M, Kennedy PD, Johnson JK, et al. CD8(+) T cells regulate tumour ferroptosis during cancer immunotherapy. Nature 2019;569(7755):270–4. [PubMed: 31043744]
44. Kaplan DH, Shankaran V, Dighe AS, Stockert E, Aguet M, Old LJ, et al. Demonstration of an interferon gamma-dependent tumor surveillance system in immunocompetent mice. Proc Natl Acad Sci U S A 1998;95(13):7556–61. [PubMed: 9636188]
45. Yoshihama S, Roszik J, Downs I, Meissner TB, Vijayan S, Chapuy B, et al. NLRC5/MHC class I transactivator is a target for immune evasion in cancer. Proc Natl Acad Sci U S A 2016;113(21):5999–6004. [PubMed: 27162338]
46. Katlinski KV, Gui J, Katlinskaya YV, Ortiz A, Chakraborty R, Bhattacharya S, et al. Inactivation of Interferon Receptor Promotes the Establishment of Immune Privileged Tumor Microenvironment. Cancer Cell 2017;31(2):194–207. [PubMed: 28196594]

47. Kalbasi A, Ribas A. Tumour-intrinsic resistance to immune checkpoint blockade. Nat Rev Immunol 2020;20(1):25–39. [PubMed: 31570880]

48. Tumbarello DA, Waxse BJ, Arden SD, Bright NA, Kendrick-Jones J, Buss F. Autophagy receptors link myosin VI to autophagosomes to mediate Tom1-dependent autophagosome maturation and fusion with the lysosome. Nat Cell Biol 2012;14(10):1024–35. [PubMed: 23023224]

49. Bach EA, Aguet M, Schreiber RD. The IFN gamma receptor: a paradigm for cytokine receptor signaling. Annu Rev Immunol 1997;15:563–91. [PubMed: 9143700]

50. Kryczek I, Lin Y, Nagarsheth N, Peng D, Zhao L, Zhao E, et al. IL-22(+)CD4(+) T cells promote colorectal cancer stemness via STAT3 transcription factor activation and induction of the methyltransferase DOT1L. Immunity 2014;40(5):772–84. [PubMed: 24816405]

51. Pirker R, Pereira JR, von Pawel J, Krzakowski M, Ramlau R, Park K, et al. EGFR expression as a predictor of survival for first-line chemotherapy plus cetuximab in patients with advanced non-small-cell lung cancer: analysis of data from the phase 3 FLEX study. Lancet Oncol 2012;13(1):33–42. [PubMed: 22056021]

STATEMENT OF SIGNIFICANCE

Loss of optineurin impairs the integrity of both IFNγ- and MHC-I-signaling pathways via palmitoylation-dependent IFNGR1 lysosomal sorting and degradation, thereby driving immune evasion and intrinsic immunotherapy resistance in colorectal cancer. Our work suggests that pharmacologically targeting IFNGR1-palmitoylation can stabilize IFNGR1, enhance T cell-immunity, and sensitize checkpoint therapy in colorectal cancer.

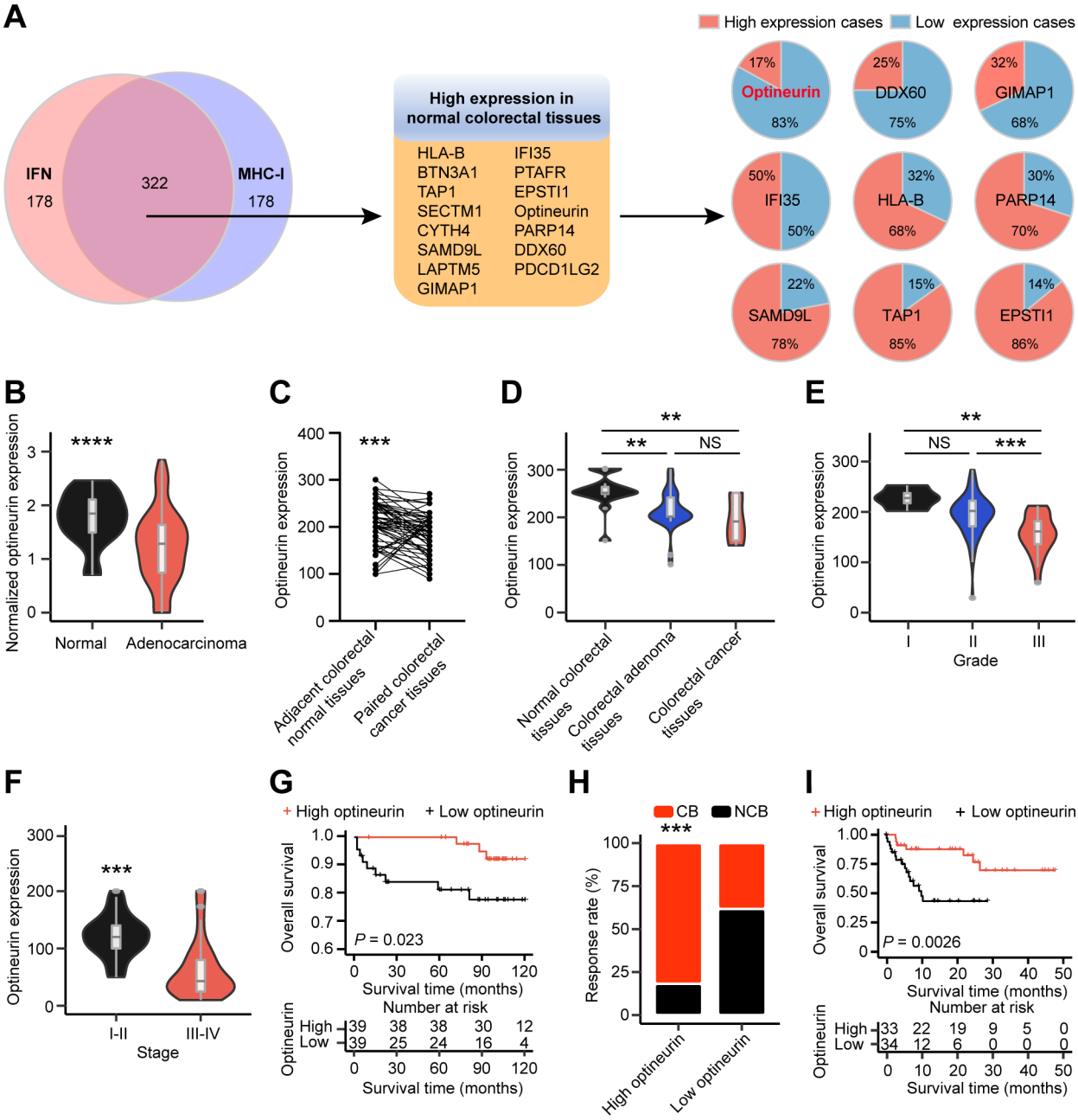

Figure 1. Tumor optineurin correlates with immunotherapy efficacy and patient outcome

A, Overlapping genes between the IFNγ- and MHC-I signaling pathways in human colorectal cancer in TCGA data set. (Left panel) Based on log FC > 0 and *P* values, top individual genes (500) and shared genes (322) were identified in the IFN-signaling and MHC-I signatures in TCGA data set. (Middle panel) Among the shared 322 genes, based on protein expression score in The Human Protein Atlas, 15 proteins with high expression score were identified in normal colorectal tissues. (Right panel) Proteomic analysis detected 9 out of 15 proteins in the paired colon cancer tissues and adjacent normal colon tissues. Sector graph represents the percentage of clinical cases with high and low expression of indicated proteins in colon cancer tissues, relative to paired adjacent normal colon tissues (n = 96).

B and **C,** Optineurin protein expression in normal colorectal tissues and colorectal cancer tissues. (**B**) Optineurin protein expression in normal colorectal tissues (n = 30) and colorectal adenocarcinoma tissues (n = 90) based on proteogenomic analysis. Two tailed t-tests, ****$P < 0.0001$. (**C**) Optineurin expression detected by immunohistochemistry staining in colorectal cancer tissues and paired adjacent normal colorectal tissues (cohort 1) (n = 66). Optineurin expression was quantified by H-score method. Paired t-tests, ***$P < 0.001$

D, Optineurin protein expression determined by immunohistochemistry staining in normal colorectal tissues (n = 16), colorectal adenoma tissues (n = 35), and colorectal cancer tissues (n = 9) (cohort 2). Optineurin expression was quantified by H-score method. Two tailed t-tests, **$P < 0.01$. *NS*: not significant. $P = 0.1741$.

E, Optineurin expression in different histological grades of colorectal cancer (n = 92) (cohort 1). Two tailed t-tests, **$P < 0.01$, ***$P < 0.001$. NS: not significant. $P = 0.1067$.

F and **G,** Optineurin protein expression detected by immunohistochemistry staining in colorectal cancer tissues (cohort 3) (n = 78). (**F**) Optineurin expression in early (I and II) versus late (III and IV) TNM stages in colorectal cancer. Two tailed t-tests, ***$P < 0.001$. (**G**) Survival was analyzed and compared between patients with low (n = 39) and high (n = 39) levels of optineurin in colorectal cancer. Log-rank test.

H and **I,** Relationship between optineurin protein expression and immunotherapy efficacy in melanoma patients. (**H**) The clinical response rates to anti-PD-1 therapy in melanoma patients with high and low optineurin expression are shown. Clinical beneficial group (CB), including complete response (CR) (n = 10) and partial response (PR) (n = 30); No clinical beneficial group (NCB), including progressive disease (PD) (n = 27). Chi-square test, ***$P < 0.001$. (**I**) Survival was analyzed and compared between patients with low (n = 34) and high (n = 33) levels of optineurin in melanoma patients treated with anti-PD-1 therapy. Log-rank test.

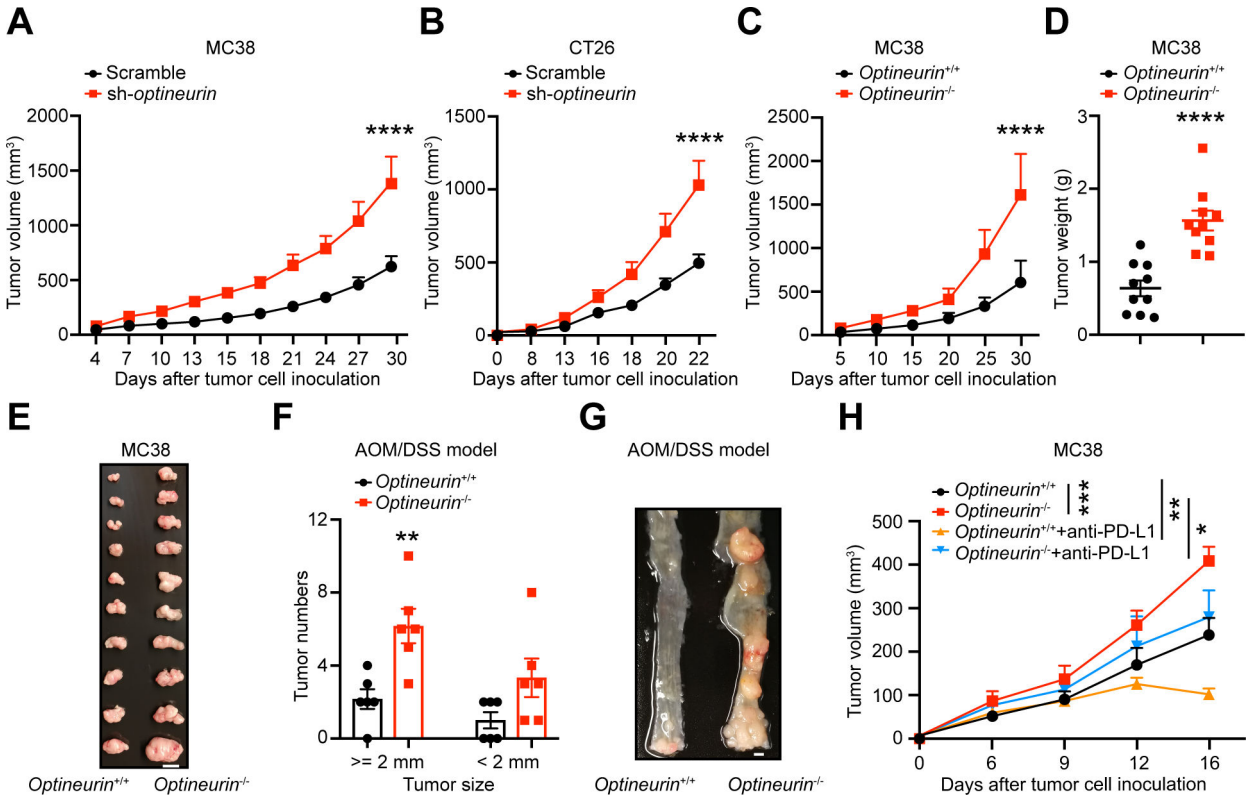

Figure 2. Optineurin affects tumor immunity and immunotherapy efficacy

A and **B,** Effect of *optineurin* knocking down on murine colorectal tumor growth. Tumor growth was monitored in syngeneic wild type mice bearing scramble and sh-*optineurin* expressing MC38 cells (**A**) and CT26 cells (**B**). Mean ± SEM. n = 8 or 9 /group (**A**) and n = 10 /group (**B**). ****$P < 0.0001$ on day 30 (**A**) and day 22 (**B**) (two-way ANOVA).

C - E, Effect of *optineurin* knock out (*optineurin*$^{-/-}$) on MC38 tumor growth. Tumor growth was monitored in C57/BL6 wild type mice bearing *optineurin*$^{+/+}$ and *optineurin*$^{-/-}$ MC38 cells. Tumor volume (**C**), weight (**D**), and images (**E**) are shown. Mean ± SEM, n = 10 / group. **** $P < 0.0001$ on day 30 (two-way ANOVA). Scale bars,1 cm (**E**).

F and **G**, Effect of IEC-*optineurin* knock-out on murine colorectal tumorigenesis in AOM/DSS model. Tumor numbers, size (**F**), and images (**G**) are shown. n = 6 /group. Two tailed t-test, **$P < 0.01$. Scale bars, 2 mm (**G**).

H, Effect of *optineurin* knock out on immunotherapy efficacy in MC38 tumor bearing mice. Mice bearing *optineurin*$^{+/+}$ and *optineurin*$^{-/-}$ MC38 tumors were treated with anti-PD-L1 mAb. *$P < 0.05$, **$P < 0.01$, ***$P < 0.01$ on day 16 (two-way ANOVA).

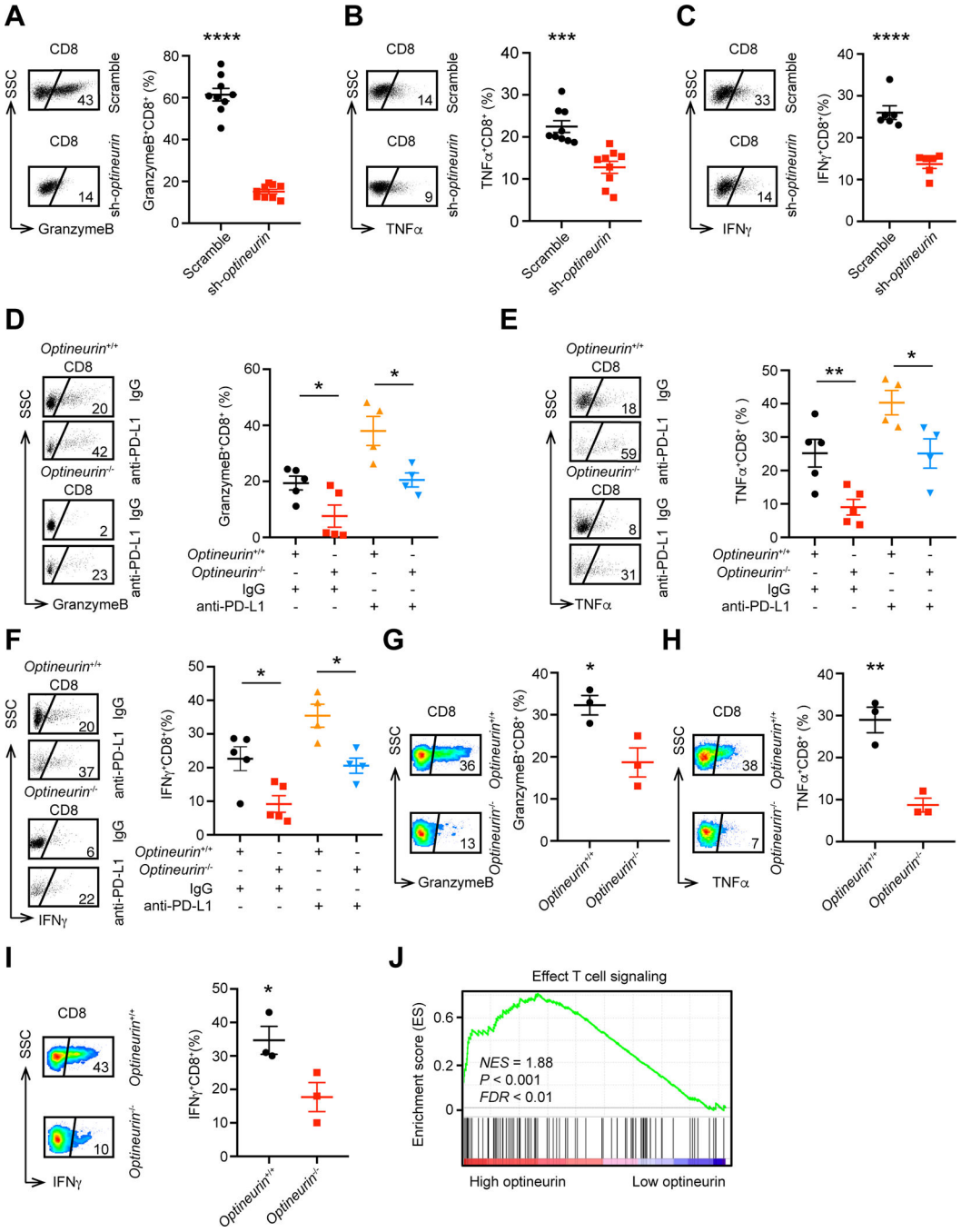

Figure 3. Optineurin impacts cytotoxic T cell activation and function *in vivo*

A - C, Effect of tumor *optineurin* knocking down on CT26 tumor infiltrating T cell function. Sh-*optineurin* and scrambled shRNA expressing CT26 cells were inoculated into BALB/c mice. The percentages of tumor infiltrating granzyme B$^+$ (**A**), TNFα$^+$ (**B**), and IFNγ$^+$ (**C**) CD8$^+$ T cells were analyzed by flow cytometry. Mean ± SEM, n = 9 /group. Two tailed t-tests, ***$P < 0.001$, ****$P < 0.0001$.

D - F, Effect of tumor optineurin deficiency on MC38 tumor infiltrating T cell function. *Optineurin*$^{+/+}$ and *optineurin*$^{-/-}$ expressing MC38 cells were inoculated into C57/BL6 mice.

The percentages of tumor infiltrating granzyme B^+ (**D**), $TNF\alpha^+$ (**E**), and $IFN\gamma^+$ (**F**) $CD8^+$ T cells were analyzed by flow cytometry. Mean ± SEM, n = 4–5 /group. Two tailed t-tests, $*P < 0.05$, $**P < 0.01$.

G - I, Effect of IEC-*optineurin* deficiency on T cell function in AOM/DSS model. The percentages of granzyme B^+ (**G**), $TNF\alpha^+$ (**H**), and $IFN\gamma^+$ (**I**) $CD8^+$ T cells in LPMCs were analyzed by flow cytometry. n = 3 /group. Two tailed t-tests, $*P < 0.05$, $**P < 0.01$.

J, Correlation of optineurin protein expression with effector T cell signaling signature in melanoma patients treated with anti-PD1 therapy (n = 67).

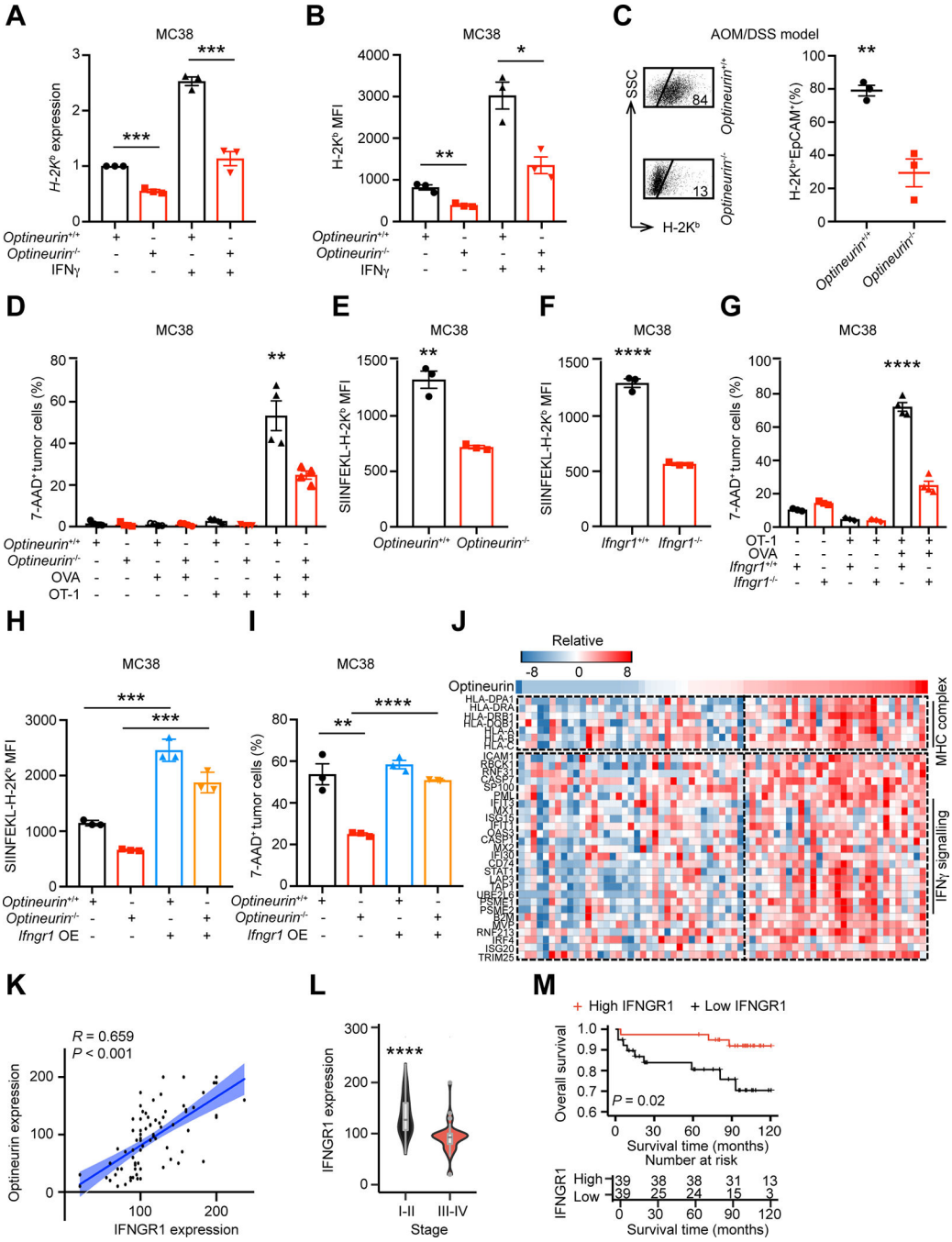

Figure 4. Optineurin deficiency impairs IFNGR1 expression and antigen presentation

A and **B,** Effect of optineurin deficiency on H-2K^b expression in MC38 cells. *Optineurin*$^{+/+}$ and *optineurin*$^{-/-}$ MC38 cells were treated with IFN**γ** for 24 hours. (**A**) *H-2K^b* mRNAs were quantified by qRT-PCR. Mean ± SEM, two tailed t-tests, ***$P < 0.001$. (**B**) H-2K^b protein expression was determined by flow cytometry analysis. Results are shown as mean fluorescence intensity (MFI). Mean ± SEM, two tailed t-tests, *$P < 0.05$, **$P < 0.01$.

C, Effect of IEC-optineurin deficiency on H-2K^{b} expression in AOM/DSS model. The percentages of H-2K^{b+} epithelial cellswere analyzed by flow cytometry. Mean ± SEM, n = 3 /group. Two tailed t-tests. $^{**}P < 0.01$.

D, Effect of tumor optineurin expression on OT-I-mediated tumor killing. OVA expressing *optineurin*$^{+/+}$ and *optineurin*$^{-/-}$ MC38 cells were co-cultured with OT-I cells for 24 hours. Tumor cell apoptosis was determined by flow cytometry analysis. Results are shown as the percentages of 7-AAD^{+} tumor cells. n = 3 biological replicates. Mean ± SEM, two tailed t-tests, $^{**}P < 0.01$.

E, Effect of tumor optineurin expression on SIINFEKL-H-2K^{b} complex. SIINFEKL-H-2K^{b} expression was quantified by flow cytometry on OVA-expressing *optineurin*$^{+/+}$ or *optineurin* $^{-/-}$ MC38 cells. Results are expressed as MFI. Mean ± SEM, two tailed t-tests, $^{**}P < 0.01$.

F, Effect of tumor Ifngr1 expression on SIINFEKL- H-2K^{b} complex. SIINFEKL- H-2K^{b} expression on OVA-expressing *Ifngr1*$^{+/+}$ or *Ifngr1*$^{-/-}$ MC38 cells was quantified by flow cytometry. Results are expressed as MFI. Mean ± SEM, two tailed t-tests, $^{****}P < 0.0001$.

G, Effect of tumor Ifngr1 expression on OT-I-mediated tumor killing. OVA expressing *Ifngr1*$^{+/+}$ and *Ifngr1* $^{-/-}$ MC38 cells were co-cultured with OT-I cells for 24 hours. Tumor cell apoptosis was determined by flow cytometry analysis. Results are shown as the percentages of 7-AAD^{+} tumor cells. n = 3 biological replicates. Mean ± SEM, two tailed t-tests, $^{****}P < 0.0001$.

H, Effect of tumor Ifngr1 on SIINFEKL- H-2K^{b} complex in *optineurin*$^{-/-}$ MC38 cells. SIINFEKL- H-2K^{b} expression on OVA-expressing *optineurin*$^{+/+}$ or *optineurin*$^{-/-}$ MC38 cells with or without ectopic *Ifngr1* expression was quantified by flow cytometry. Results are expressed as MFI. n = 3 biological replicates. Mean ± SEM, two tailed t-tests, $^{***}P < 0.001$.

I, Effect of tumor Ifngr1 expression on OT-I-mediated tumor killing in *optineurin*$^{-/-}$ MC38 cells. OVA expressing *optineurin*$^{+/+}$ and *optineurin*$^{-/-}$ MC38 cells with or without ectopic *Ifngr1* expression were co-cultured with OT-I cells for 24 hours. Tumor cell apoptosis was determined by flow cytometry analysis. Results are shown as the percentages of 7-AAD^{+} tumor cells. n = 3 biological replicates. Mean ± SEM, two tailed t-tests, $^{**}P < 0.01$, $^{****}P < 0.0001$.

J, Correlation of optineurin protein expression with the MHC complex and IFNγ-signaling genes. Heatmap shows MHC complex proteins and IFNγ-signaling proteins in melanoma patients treated with anti-PD1 therapy (n = 67). Each color represents differential gene expression: red represents high expression; blue represents low expression.

K, Correlation of optineurin and IFNGR1 protein expression in colorectal cancer tissues. Pearson correlation analysis. Expression of optineurin and IFNGR1 was determined by immunohistochemistry and expressed as H-score. Cohort 3, n = 78.

L and **M,** Pathological and clinical impact of tumor IFNGR1 protein on patients with colorectal cancer. IFNGR1 protein was examined by immunohistochemistry staining. (**L**) IFNGR1 expression in different stages of colorectal cancer patients. Cohort 3, n = 78, two tailed t-tests, $^{****}P < 0.0001$. (**M**) Survival was analyzed and compared between patients with low (n = 39) and high (n = 39) levels of IFNGR1 in colorectal cancer. Log-rank test. Cohort 3, n = 78.

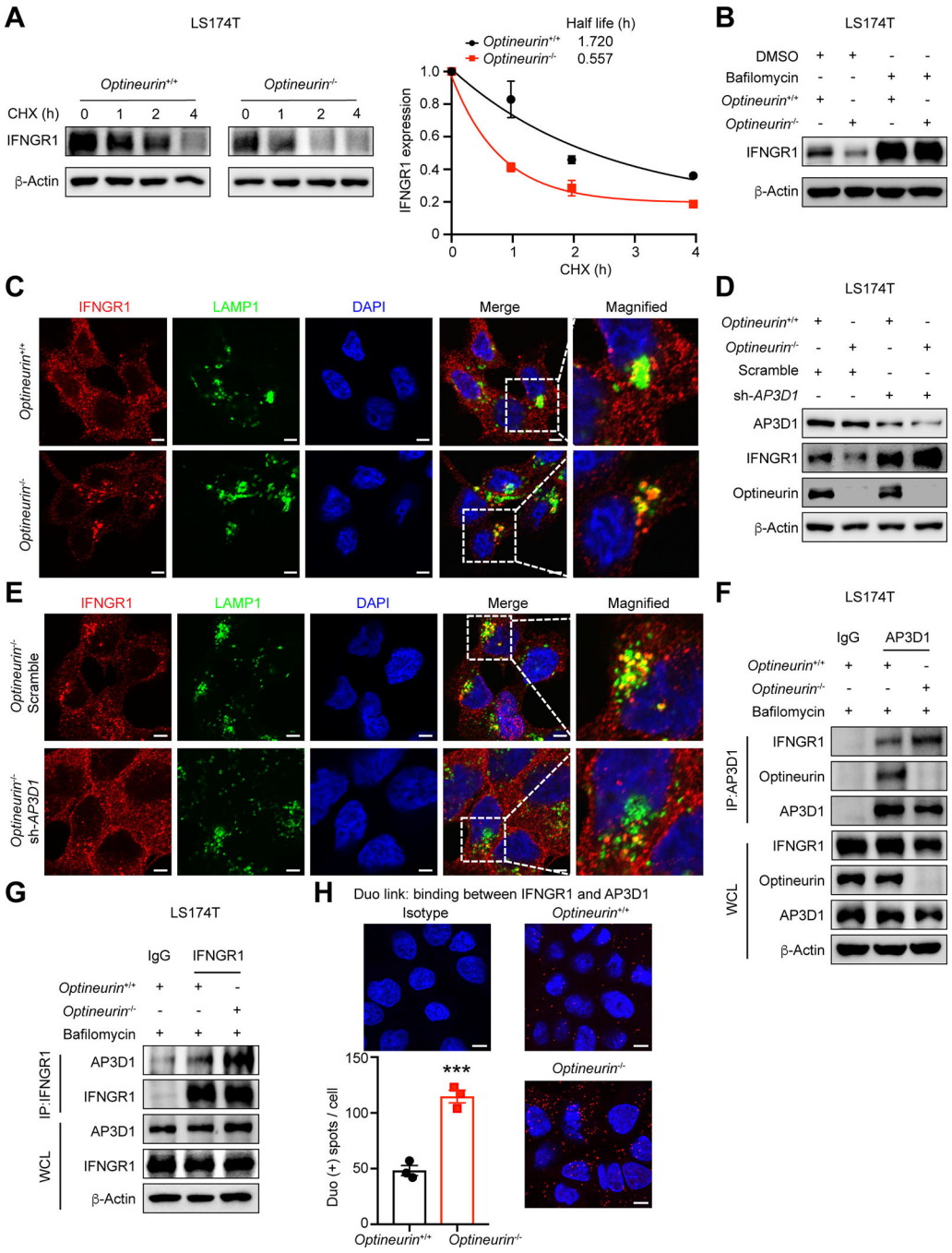

Figure 5. Loss of optineurin promotes IFNGR1 lysosomal sorting via AP3D1

A - C, Role of optineurin in IFNGR1 degradation. (**A**) *Optineurin*$^{+/+}$ and *optineurin*$^{-/-}$ LS174T cells were treated with cycloheximide (CHX). Immunoblots revealed IFNGR1 expression bands (left) and relative band intensities (right) at different time points. One of 3 replicates is shown. (**B**) *Optineurin*$^{+/+}$ and *optineurin*$^{-/-}$ LS174T cells were treated with Bafilomycin for 4 hours. Immunoblots showed IFNGR1 expression. One of 3 replicates is shown. (**C**) Effect of optineurin on tumor IFNGR1 lysosomal localization. *Optineurin*$^{+/+}$ and *optineurin*$^{-/-}$ DLD1 cells were stained for IFNGR1 (Red) and LAMP1 (Green). Cell nucleus

(Blue) was stained with 4′,6-diamidino-2-phenylindole (DAPI). Representative immunofluorescence images exhibit the co-localization of IFNGR1 and LAMP1. Scale bars, 5 μm. n = 3 biological replicates.

D, Effect of AP3D1 on IFNGR1 expression. IFNGR1 expression in sh-*AP3D1* and scrambled shRNA expressing *optineurin*$^{+/+}$ and *optineurin*$^{-/-}$ LS174T cells. Immunoblots showed IFNGR1 expression. n = 3 biological replicates.

E, Effect of AP3D1 on IFNGR1 localization. IFNGR1 (Red) and LAMP1 (Green) stained in sh-*AP3D1* and scrambled shRNA expressing *optineurin*$^{-/-}$ DLD1 cells. Representative immunofluorescence images exhibit the co-localization of IFNGR1 and LAMP1. Cell nucleus (Blue) was stained with DAPI. Scale bars, 5 μm. n = 3 biological replicates.

F - H, Effect of optineurin expression on the interaction between IFNGR1 and AP3D1. (**F** and **G**) Detection of endogenous IFNGR1 and AP3D1 binding by Co-IP. Proteins in *optineurin*$^{+/+}$ and *optineurin*$^{-/-}$ LS174T cells were immunoprecipitated using anti-AP3D1 antibody (**F**) or anti-IFNGR1 antibody (**G**), and immunoblotted using anti-IFNGR1 and anti-AP3D1. Cells were treated with Bafilomycin (100 μM) for 4 hours. Whole-cell lysate (WCL). n = 3 biological replicates. (**H**) Detection of endogenous IFNGR1 and AP3D1 binding (red dots) by Duolink assay. The number of red dots was divided by the number of nuclei. Three biological replicates were performed. Scale bar, 7 μm. Mean ± SEM, two tailed t-tests, *** $P < 0.001$.

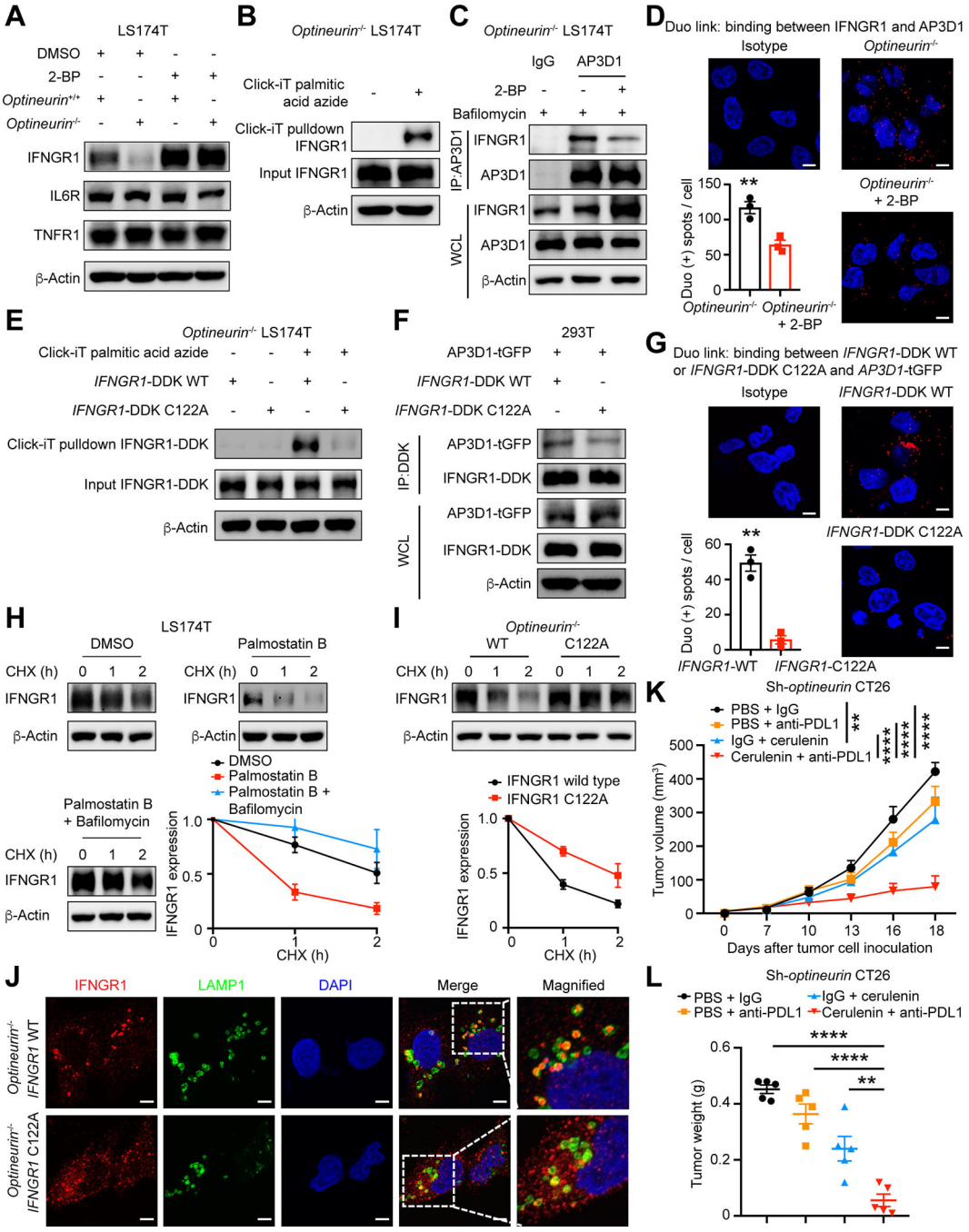

Figure 6. IFNGR1 palmitoylation alters the IFNGR1-AP3D1 interaction and tumor immunity

A, Effect of 2-BP on IFNGR1, IL6R, and TNFR1 expression in LS174T cells. *Optineurin*$^{+/+}$ and *optineurin*$^{-/-}$ LS174T cells were treated with 2-BP for 4 hours. IFNGR1, IL6R, and TNFR1 expression was detected by immunoblots. One of 3 experiments is shown.

B, Detection of IFNGR1 palmitoylation in *optineurin*$^{-/-}$ LS174T cells. *Optineurin*$^{-/-}$ LS174T cells were treated and prepared for the Click-iT reaction. One of 3 replicates is shown.

C and **D,** Effect of 2-BP on the interaction between IFNGR1 and AP3D1. (**C**) Detection of endogenous IFNGR1 and AP3D1 binding by Co-IP. *Optineurin*$^{-/-}$ LS174T cells were treated with or without 2-BP and Bafilomycin for 4 hours. Proteins were collected from these cells and were immunoprecipitated using AP3D1 antibody and immunoblotted using anti-IFNGR1. Whole-cell lysate (WCL). n = 3 biological replicates. (**D**) Detection of endogenous IFNGR1 and AP3D1 binding (red dots) by Duolink assay. *Optineurin*$^{-/-}$ DLD1 cells were treated with or without 2-BP for 2 hours. The number of red dots was divided by the number of nuclei. Three biological replicates were performed. Scale bar, 7 μm. Two tailed t-tests, ** $P < 0.01$.

E, Identification of IFNGR1 palmitoylation site. *Optineurin*$^{-/-}$ LS174T cells were ectopically expressed with wild type *IFNGR1*-DDK (WT) or *IFNGR1* C122A mutant -DDK (C122A) plasmid, and treated and prepared for the Click-iT reaction. One of 3 replicates is shown.

F and **G**, Effect of C122A mutation on the interaction between IFNGR1 and AP3D1. (**F**) Detection of the interaction of IFNGR1 and AP3D1 by Co-IP. 293T cells were transfected with *AP3D1*-tGFP plasmid, *IFNGR1*-DDK wild type (WT) plasmid, or *IFNGR1*-DDK C122A mutant plasmid. Proteins were isolated from these cells, immunoprecipitated using anti-DDK antibody, and immunoblotted using anti-tGFP. n = 3 biological replicates. (**G**) Detection of the interaction (red dots) of AP3D1 with *IFNGR1*-WT or *IFNGR1*-C122A by Duolink assay. *Optineurin*$^{-/-}$ DLD1 cells were transfected with *AP3D1*-tGFP plasmid, *IFNGR1*-DDK WT plasmid, or *IFNGR1*-DDK C122A mutant plasmid for 48 hours. The number of red dots was divided by the number of nuclei. Three biological replicates were performed. Scale bar, 7 μm. Two tailed t-tests, ** $P < 0.01$.

H, Effect of palmitoylation on IFNGR1 degradation in LS174T cells. LS174T cells were treated with CHX in the presence of Palmostatin B and Palmostatin B plus Bafilomycin. Immunoblots showed IFNGR1 protein expression bands and band intensity at different time points. One of 3 experiments is shown.

I, Effect of C122A mutation on IFNGR1 stability in LS174T cells. *Optineurin*$^{-/-}$ LS174T cells were ectopically expressed with WT *IFNGR1*-DDK or *IFNGR1* C122A-DDK plasmid, and cultured with CHX. Immunoblots showed IFNGR1-DDK band and band intensities at the indicated time points. One of 3 replicates is shown.

J, Effect of C122A mutation on tumor IFNGR1 lysosomal localization. *Optineurin*$^{-/-}$ DLD1 cells were ectopically expressed with wild type *IFNGR1* or C122A mutants, and stained for IFNGR1 (Red) and LAMP1 (Green). Representative immunofluorescence images showed the co-localization of IFNGR1 and LAMP1. Cell nucleus (Blue) was stained with DAPI. Scale bars, 5 μm. n = 3 biological replicates.

K and **L,** Effect of cerulenin and anti-PD-L1 mAb therapy on colon tumor progression. Mice bearing sh-*optineurin* CT26 tumor was treated with cerulenin, anti-PD-L1, or their combination. Tumor volume (**K**) and weight (**L**) are shown. Mean ± SEM, n = 5 /group. ** $P < 0.01$, **** $P < 0.0001$ on day 18 (two-way ANOVA).